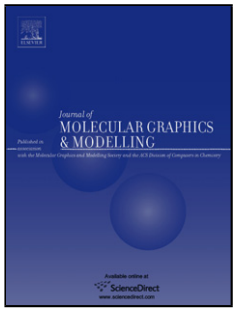

Title: Molecular Dynamics Simulation and Free Energy Calculation Studies of Kinase Inhibitors Binding to Active and Inactive Conformations of VEGFR-2

Author: XiaoYun Wu ShanHe Wan GuangFa Wang Hong Jin ZhongHuang Li YuanXin Tian ZhengGuang Zhu JiaJie Zhang

PII: S1093-3263(14)00209-5
DOI: http://dx.doi.org/doi:10.1016/j.jmgm.2014.12.006
Reference: JMG 6500

To appear in: *Journal of Molecular Graphics and Modelling*

Received date: 12-5-2014
Revised date: 4-12-2014
Accepted date: 16-12-2014

Please cite this article as: X.Y. Wu, S.H. Wan, G.F. Wang, H. Jin, Z.H. Li, Y.X. Tian, Z.G. Zhu, J.J. Zhang, Molecular Dynamics Simulation and Free Energy Calculation Studies of Kinase Inhibitors Binding to Active and Inactive Conformations of VEGFR-2, *Journal of Molecular Graphics and Modelling* (2014), http://dx.doi.org/10.1016/j.jmgm.2014.12.006

Highlights

1. MM-GBSA and MM-PBSA calculations verify that inhibitors **1** and **2** have almost the same activities against VEGFR-2.
2. The decomposition of binding free energy into each interaction type suggests that van der Waals interactions provided the substantial driving force for the binding process.
3. The important hydrophobic property of the terminal 4-Cl phenyl was required to be type II inhibitors.

*Corresponding author

XiaoYun Wu, JiaJie Zhang

Tel: +86-20-62789416; Fax: +86-20-61648548

E-mail: xywugz@163.com (X.Y. Wu), zhangjj@smu.edu.cn(J.J. Zhang)

Molecular Dynamics Simulation and Free Energy Calculation Studies of Kinase Inhibitors Binding to Active and Inactive Conformations of VEGFR-2

XiaoYun Wu*, ShanHe Wan, GuangFa Wang, Hong Jin, ZhongHuang Li, YuanXin Tian, ZhengGuang Zhu, JiaJie Zhang*

School of Pharmaceutical Sciences, Southern Medical University, Guangzhou 510515, PR China

Abstract

Vascular endothelial growth factors receptor-2 (VEGFR-2) inhibitors have been proved as very effective anticancer agents. Structurally similar ligands **1** and **2** show almost the same inhibitory activities against VEGFR-2, but they bind to the enzyme in distinct binding mode. Ligand **1** targets DFG-in active conformation of VEGFR-2, known as Type I inhibitor. On the other hand, ligand **2** targets DFG-out inactive conformation of VEGFR-2, known as Type II inhibitor or allosteric kinase inhibitor. Ligand **2** shows high inhibitory activity, while the compound **3**, a close analog of **2** with the cyclopropylamide replaced by tert-butylamide, exhibits drastically diminished potency. In this work, molecular dynamics simulations and free energy calculations were performed on inhibitors **1**-**3** binding to active and inactive conformation of VEGFR-2. Molecular dynamics simulations find that the active conformation binding to Type I inhibitor **1** appears more flexible when compared to the unbound form. In contrast, binding of Type II inhibitor **2** to the inactive conformation helps to stabilize the inactive conformation of the protein. Binding free energy calculations verify that inhibitor **1** and **2** have almost the same activities against VEGFR-2, and that ligand **1** binds to and stabilizes the DFG-in conformation of VEGFR-2, which is in agree with the experimental observation. Molecular dynamics simulations and binding free energy calculations of **3** binding to VEGFR-2 can give a good explanation of the drastically diminished potency. Free energy analysis revealed that van der Waals interactions provided the substantial driving force for the binding process. The important hydrophobic property of the terminal 4-Cl phenyl was required to be type II inhibitors. Furthermore, per-residue free energy decomposition analysis revealed that the most favorable contribution came from Leu840, Val848, Ala866, Lys868, Leu889, Val899, Thr916, Phe918, Cys919, Leu1035, Cys1045, Asp1046, and Phe1047. These results are expected to be useful for future rational design of novel potent VEGFR-2 inhibitors.

Keywords: VEGFR-2, Type I inhibitors, Type II inhibitors, Molecular dynamics, MM-PBSA, MM-GBSA

1. Introduction

Vascular endothelial growth factors (VEGFs) play a very important role in the regulation of angiogenesis, the process that lead to the formation of new blood vessels [1-2]. Abnormal regulation of angiogenesis has been shown to get involved in many diseases, such as diabetic retinopathy, psoriasis, rheumatoid arthritis, and cancer. Particularly, it is widely recognized that the growth and metastasis of solid tumors is dependent on angiogenesis [3-4]. The VEGFs exert its effects through receptor tyrosine kinase (VEGFR-1, -2, and -3). Among them, VEGF receptor-2 (VEGFR-2) plays crucial roles in vessel sprouting and new vessel initiation in early stage of angiogenesis.

It is well established that inhibiting of VEGFR-2 leads to suppression of angiogenesis and tumor growth. A number of preclinical and clinical studies have shown that many small-molecule VEGFR-2 inhibitors are capable of inhibiting angiogenesis, tumor progression, and dissemination [5-9]. Most kinase inhibitors discovered to date are ATP-competitive and classified as type I inhibitors. Such inhibitors target the ATP binding pocket in its active conformation of the activation loop. This conformation is normally referred to as DFG-in based on the position of the conserved triad aspartate-phenylalanine-glycine (DFG) at the entrance of the activation loop. Type I inhibitors typically function in the DFG-in conformation of VEGFR-2 through hydrogen bonding with the hinge region as well as hydrophobic interactions in and around the adenine region. On the other hand, type II inhibitors bind to and stabilize an inactive kinase form that features the DFG motif in a DFG-out conformation. The different position of the DFG residues in the DFG-out form creates a new hydrophobic binding pocket that is adjacent to the ATP-binding site. This pocket, also known as the allosteric site, is characteristic of kinase in an inactive conformation. Type II inhibitors predominantly occupy the ATP binding site, but they also exploit unique hydrogen bonding and hydrophobic interactions with the allosteric site. Compared with type I kinase inhibitors, type II inhibitors have several advantages, including great cellular potency and improved kinase selectivity [10-15]. Therefore, DFG-out conformation has gained great interest in discovery and development of type II kinase inhibitors for the past few years. However, problems pursuing this type of inhibitor also exist. Mutations at or around allosteric pocket are more likely to occur that at evolutionary conserved regions, potentially leading problems associated with drug-resistance.

Recently, Amgen Inc. reported a dimethoxyyquinoline template targeting the hinge region of VEGFR-2 [16,

17]. The X-ray co-crystal structure of VEGFR-2 in complex with Ligands **1** and **2** were reported . Ligands **1** and **2** (Fig.1) with the same scaffold and similar substituents bind to the enzyme in distinct DFG-in and DFG-out mode, respectively. Accordingly, ligands **1** and **2** were classified as type I and type II inhibitors, respectively. Despite the difference in the binding mode, ligands **1** and **2** show almost the same inhibitory activities against VEGFR-2. Ligand **2** is a potent inhibitor, while the compound **3**, a close analog of **2** with the cyclopropylamide replaced by tert-butylamide, exhibits drastically diminished potency. To improve our understanding of the structural determinants for type I and II kinase inhibitors binding to and stabilizing the DFG-in and DFG-out conformation, a combined computational approach by molecular dynamics (MD) simulations, molecular mechanics Poisson-Boltzmann surface area (MM-PBSA) and molecular mechanics/generalized Born surface area (MM-GBSA) free energy calculations and MM-GBSA free energy decomposition analysis was performed in the present study. We investigated type I inhibitor **1** binding to active conformations and type II inhibitor **2** binding to inactive conformations. For comparison, we also investigated **1** binding to the inactive conformation, compound **3** binding to active and inactive conformations, and the unbound forms of both protein conformations. We expect that this study will be helpful for the rational design of VEGFR-2 kinase inhibitors.

2. Materials and Methods

2.1. Initial Structure Preparation

The atomic coordinates of the crystal structure for ligands **1** and **2** in complex with VEGFR-2 in active and inactive conformations were retrieved from the protein data bank (PDB entries: 3B8R, and 3B8Q, respectively)[16,17] . The structures are in a dimer former, only one chain is kept. The complex protein structure models were created by removing all ions, and all water molecules. The regions encompassing residues 842-846, 1050-1066 in 3B8R, and 1048-1066 in 3B8Q, not solved in the crystal structures, were modeled using the loop building routine in Modeler [18]. The reliability of the generated model was evaluated by QMEAN4 scoring function (Fig. S1 in supporting information) [19].The 3B8R and 3B8Q based models are henceforth referred to as **1**-VEGFR-2(active) and **2**-VEGFR-2(inactive), respectively. A model of **1** binding to the inactive conformation of VEGFR-2 was generated for the purpose of comparison. This model was created by replacing ligand **2** with **1** in the inactive 3B8Q based VEGFR-2 model. Superposition of the ligands was performed based on the 3B8R-3B8Q Cα-atom alignment. This structure is termed as **1**-VEGFR-2(inactive). No model of **2** bound to the active VEGFR-2 conformation was generated as the absence of the back-pocket prevents the inhibitor

from binding. The models of **3**-VEGFR-2(active) and **3**-VEGFR-2(inactive) were prepared by modifying the structure of compound **1** using the sketch module of Sybyl 7.3[20]. Unbound structures of the active and inactive VEGFR-2 conformations were created by removing the ligands from the **1**-VEGFR-2(active) and **2**-VEGFR-2(inactive) models, respectively. These models are termed as VEGFR-2(active, unbound) and VEGFR-2(inactive, unbound) models, respectively. The treated structures were used as the initial structures of MD simulation.

Geometry optimization and the electrostatic potential calculations for compounds **1-3** were performed at the HF/6-31G* level of the Gaussian03 suite [21]. The atomic partial charge of the three ligands was obtained by using RESP fitting method [22] implemented in AmberTools [23]. The force field parameters for the ligands were generated by the general amber force field (GAFF) [24] using the Antechamber program. The AMBER 99SB force field [25] was used to simulate all protein structures and the ionization state of amino acid residues was set according to the standard protocol. All models were neutralized by adding suitable counterions and were solvated in a truncated octahedron box of TIP3P [26] water molecules with a margin distance of 12 Å.

2.2. MD Simulation

The MD simulations were performed using the PMEMD module of AMBER 12 software package [27, 28]. Initially, the solvated systems used as the starting structure for subsequent MD simulations were minimized by three steps. First, a harmonic constraint potential of 2.0 kcal·mol^{-1}·Å^{-2} was applied to all the protein atoms. Second, the protein backbone atoms were restrained with a force of 2.0 kcal·mol^{-1}·Å^{-2}. Third, all atoms were allowed to move freely. In each step, energy minimization was executed by the steepest descent method for the first 4000 steps and the conjugated gradient method for the subsequent 1000 steps. After minimization, the MD simulations performed in this study followed a standard protocol consisting of gradual heating, density equilibration, equilibration, and production procedures. Firstly, the systems were gradually heated in the NVT ensemble from 0 to 300 K in 50 ps using a Langevin thermostat with a coupling coefficient of 1.0/ps with a force constant 2.0 kcal·mol^{-1}·Å^{-2} on the complex. And then 50 ps of density equilibration with a force constant 2.0 kcal·mol^{-1}·Å^{-2} on the complex were performed. Subsequently the systems were again equilibrated for 1 ns by releasing all the restrains. Finally, the actual MD production run of 80 ns in the NPT ensemble for each system was performed at 300 K with 1.0 atm pressure. During the MD simulations, the long-range Coulombic interactions were handled using the particle mesh Ewald (PME) method [29]. The cutoff distance for the

long-range van der Waals (vdW) energy term was set at 10.0 Å. Periodic boundary conditions were applied to avoid edge effects in all calculations. The SHAKE algorithm [30] was employed on all atoms covalently bond to hydrogen atoms, allowing for an integration time step of 2 fs. Coordinate trajectories were recorded every 10 ps throughout all equilibration and production runs, and 1000 snapshots of the simulated structures within the last 10 ns stable MD trajectory at 10 ps intervals were extracted to perform the following binding free energy calculations.

2.3. Binding Free Energy Calculations

The binding free energies (ΔG_{bind}) of the inhibitors with VEGFR-2 were calculated by using MM-PB/GBSA [31] procedure in AMBER12. Average 1000 snapshots were extracted from the last 10 ns MD trajectory for the calculations. The single trajectory approach was applied to estimate the energies, as estimation of energies in this manner has proven successful in many studies. A part of the reason for the success of this approach is the cancelation of errors that hides the effect of incomplete sampling. The binding free energy is computed for each molecular species (complex, protein, and ligand) as the difference:

$\Delta G_{bind}=G_{complex} - (G_{protein}+G_{ligand})$

Each term can be estimated as follows:

$\Delta G = \Delta G_{MM}+ \Delta G_{sol} - T\Delta S$

Where ΔG_{MM} is the molecular mechanics free energy, ΔG_{sol} is the solvation free energy, and $T\Delta S$ represents the entropy term.

The molecular mechanics energy was calculated by the electrostatic and van der Waals interactions:

$\Delta G_{MM} =\Delta G_{ele}+ \Delta G_{vdW}$

The solvation free energy was composed of the polar and the nonpolar contributions:

$\Delta G_{sol} = \Delta G_{ele, sol} + \Delta G_{np, sol}$

Where the polar part $\Delta G_{ele,sol}$ could be calculated by solving the Poisson Boltzmann (PB) equations [32] for MM-PBSA method or generalized Born (GB) model [33] for MM-GBSA. And the parameters used for the GB calculation are developed by Onufriev et al [33]. (GB^{OBC}, igb = 2).

The nonpolar solvation contribution was determined using the solvent accessible surface area (SASA, $Å^2$) with Amber molsurf module, according to:

$\Delta G_{np, sol} = \gamma SASA+\beta$

For the surface tension (γ) and offset (β), we have considered the standard values of 0.005420 kcal·mol^{-1}·Å^{-2} and −1.008000 kcal·mol^{-1} for PB calculations and 0.0072 kcal·mol^{-1}·Å^{-2} and 0 for GB calculations, respectively. A probe radius of 1.4 Å for the solvent has been used in the SASA calculation. Dielectric constants of 1.0 and 80.0 were used for solute and solvent, respectively.

The conformational entropy (translation, rotation, and vibration) upon ligand binding, TΔS, was calculated using normal-mode analysis with the NMODE program in AMBER12. Prior to the normal-mode calculations, each snapshot was minimized for a maximum number of 100 000 cycles using the conjugate gradient method with in the presence of a distance-dependent dielectric of $4r_{ij}$ (r_{ij} is the distance between two atoms) until the root-mean-square of the elements of the gradient vector was less than 1.0×10^{-4} kcal·mol^{-1}·Å^{-1}. Due to the high computational demand of this approach, only 10 snapshots evenly extracted from the last 10 ns MD trajectory were used to calculate the entropic contribution.

2.4. Per-Residue Free Energy Decomposition Analysis

To identify the key residues responsible for the binding process of inhibitors, free energy decomposition to each residue was performed. Because of faster calculation in MM-GBSA procedure, it becomes more attractive than MM-PBSA, the interaction between inhibitor and each residue was computed using the MM-GBSA decomposition process in AMBER12. The decomposition was performed only for molecular machanics and salvation energies but not for entropies. The binding interaction of each inhibitor-residue pair includes four terms: van der Waals contribution (ΔG_{vdW}), electrostatic contribution (ΔG_{ele}), polar solvation contribution ($\Delta G_{ele,sol}$), and nonpolar solvation contribution ($\Delta G_{np,sol}$):

$$\Delta G_{inhibitor\text{-}residue} = \Delta G_{vdW} + \Delta G_{ele} + \Delta G_{ele,\,sol} + \Delta G_{np,\,sol}$$

Where the vdW and electrostatic interactions between inhibitor and per-residue of VEGFR-2 were computed using the Sander program in AMBER12. The polar contributions of the solvation free energy were calculated by using the Generalized-Born (GB) model (GB^{OBC}, igb = 2) [33]. The nonpolar contributions of the desolvation energy were determined with solvent accessible surface area (SASA) dependent terms. All energy components were calculated using 1000 snapshots extracted from the last 10 ns MD trajectory.

3. Results and Discussion

3.1. Stability of Molecular Dynamics Simulations

It is not surprising that ligands **1** and **2** with the same scaffold and similar substituents bind to the enzyme in a similar manner. The quinoline nitrogen of the two ligands form hydrogen bond interactions with the backbone NH of Cys919 in the hinge region. The naphthyl core is accommodated in the mostly hydrophobic ATP-binding cleft. The carbonyl and NH of the amide group of the two ligands make two hydrogen bond interactions with the backbone NH of Asp1046 and the side chain of Glu885, respectively. However, two crystallographic structures reveal a large conformational change in the highly conserved Asp-Phe-Gly (DFG) loop located at the start of the activation loop (Fig.2a). This conformation change, wherein Phe 1047 of DFG motifs has shifted by about 10Å, open up the extended hydrophobic pocket. When complexed with ligand **2**, VEGFR-2 adopts a DFG-out inactive kinase conformation, allowing the p-Cl phenyl ring of **2** to penetrate into the extended hydrophobic pocket. In contrast, when complexed with ligand **1**, the DFG loop is maintained in a DFG-in conformation without the extended hydrophobic pocket (Fig.2). Despite the difference in the conformations, ligands **1** and **2** show almost the same inhibitory activities against VEGFR-2. Ligand **2** is a potent inhibitor, while the compound **3**, a close analog of **2** with the cyclopropylamide replaced by tert-butylamide, exhibits drastically diminished potency.

MD simulations were performed on **1**-VEGFR-2(active) and **2**-VEGFR-2(inactive) models. For contrast, MD simulations were also performed on models of **1** bound to the inactive VEGFR-2 conformation, models of **3** bound to the active and inacitve VEGFR-2 conformations, and models of both unbound active and inactive protein conformations. MD simulations for the seven systems in explicit aqueous solution were run for duration of 80 ns. In order to ensure the rationality of the MD simulated results, we first compared the representative snapshots of each complex taken from the last 10 ns MD trajectory with the initial structure. As illustrated in Fig. 2, the binding modes of **1** and **2** from MD simulated results are nearly the same as that extracted from the X-ray co-crystal structures. Compound **1** bound to inactive conformation and compound **3** bound to active and inactive conformation also share similar binding modes with **1**.

It can reflect the dynamic stabilities of the all systems using the values of root-mean-square deviations (RMSDs) for all backbone atoms of protein, backbone atoms of residues in the binding pocket within 5 Å around each inhibitor, and all heavy atoms of each inhibitor. The RMSDs of each of seven systems relative to their starting structure were plotted in Fig. 3 and listed in table 1. As can be seen in the plots, the systems except **1**-VEGFR-2(active) and **3**-VEGFR-2(active) have similar RMSD values within 3.0 Å of the initial structures

and reached equilibrium after 10ns simulation time. From Fig. 3, the **3**-VEGFR-2(active) complex did not reached equilibrium during the 80 ns simulation time, indicating that compound **3** has an unstable binding with VEGFR-2 in DFG-in form. The **1**-VEGFR-2(active) complex shows the highest fluctuations among the other six and it took 40 ns to reach equilibrium, with average RMSDs of 3.88 Å for protein. From the unbound simulations, we can see that the RMSD of VEGFR-2(active) decreased in the unbound structure compared to the ligand bound structure and that the RMSD of VEGFR-2(inactive) increased in the unbound structure compared to the ligand bound structure (Table 1). One might therefore conclude that the active conformation binding to inhibitor shows more flexible to a degree when compared to the unbound form, whereas the inactive conformation is stabilized, at least by inhibitors such as ligand **2**, which possess a back-pocket binding group.

Table 1

The root mean square deviation (RMSD) average of the overall protein structures, active sites and ligands for the last 10 ns MD trajectories[a]

	1-VEGFR-2 (active)	**1**-VEGFR-2 (inactive)	**2**-VEGFR-2 (inactive)	**3**-VEGFR-2 (active)	**3**-VEGFR-2 (inactive)	VEGFR-2 (active, unbound)	VEGFR-2 (inactive, unbound)
Overall structure	3.88 (0.16)	2.54 (0.21)	2.51 (0.18)	3.00 (0.15)	2.29 (0.12)	2.57 (0.23)	2.87 (0.32)
Active site	1.03 (0.11)	0.75 (0.12)	0.66 (0.08)	0.85 (0.10)	1.01 (0.09)	-	-
Ligand	0.38 (0.08)	0.48 (0.11)	0.77 (0.22)	0.79 (0.18)	0.81 (0.19)	-	-

[a] Root-mean-square deviation (RMSD) average for all backbone atoms (C, Cα, and N) of protein, backbone atoms (C, Cα, and N) of active sites (residues within 5 Å around each inhibitor), and all heavy atoms of each inhibitor (Å) with standard deviation (SD) values (Å) in parenthesis.

Ligand **1** in the **1**-VEGFR-2(active) and **1**-VEGFR-2(inactive) systems and **3** in **3**-VEGFR-2(inactive) system are stable after equilibrium, with average 0.38 Å, 0.48 Å, and 0. 81 Å RMSD fluctuations, respectively. The ligand **2** exhibits different dynamics behaviors in the active site of VEGFR-2. As seen from Fig. 3, the RMSD values fluctuate around 0.60 Å during the first 17.4ns. Afterward, a sharp rise is observed and the function keeps stable with average RMSD values of 0.96 Å for about 30ns. During about 47.2 ns, a sudden drop is observed and then the function keeps stable with average RMSD values of 0.55 Å for about 20ns. During about 67.8 ns, a sharp rise is also observed and then the function keeps stable with average RMSD values of 0.96Å in the rest of the simulation. This indicates that the conformation of ligand **2** undergoes a notable change along the simulation. The average structures of ligand **2** from 17.4 to 47.2 ns and from 47.2 to 67.8 ns MD trajectories are displayed in Fig. S2 in supporting information. It is obvious that the flip has taken place in the terminal 4-Cl phenyl.

Furthermore, analyses of root-mean-square fluctuation (RMSF) versus the residue number for complexes are

illustrated in Fig. 4. For comparison, the corresponding values of RMSFs obtained from the experimental B-factors in crystal structures are also shown in Fig. 4. The experimental B-factors are transformed to the RMSF with the equation $<\Delta r_i^2>=3Bi/(8\pi^2)$ [34]. RMSF profiles indicate that the residues with higher fluctuation values are those in the flexible loops. The observations are in agreement with the experimental results reflected by the B factors derived from the X-ray crystallographic data, indicating the reasonability of our MD results. Accordingly, the protein structures of all systems share similar RMSF distributions and similar trends of dynamic features. For VEGFR-2 bound complexes, it shows relatively rigid in the active site region (residues Leu840, Val848, Val899, Thr916, Phe918, Cys919, Leu1035, Cys1045, Asp1046, and Phe1047). The fluctuation of the active site for **1**-VEGFR-2(active) complex is more significant, and **2**-VEGFR-2(inactive) complex is smallest among the five complexes. Analysis of the results from the **1**-VEGFR-2(inactive) simulation, where **1** was placed in the active site of the inactive conformation, reveals that the ligand also fluctuates to a larger degree also in this cavity. This suggests that the behavior of **1** is characteristic of the molecule itself and not an effect of the protein conformation.

The hydrogen bond plays an important role in inhibitor binding to kinase. For the five protein-inhibitor systems, the hydrogen-bond interactions with key residues in the binding pocket are listed in Table 2. A hydrogen bond is defined by distance (< 3.5Å) and orientation (the angle A···H-D > 120.0). The major interactions in the VEGFR-2 kinase-binding site is the important H-bonding interactions with the backbone of Asp1046 and Cys919. In the simulations of **1**-VEGFR-2(active) and **2**-VEGFR-2(inactive) systems, the quinoline NH of ligands **1** and **2** establish hydrogen bond interactions with backbone of Cys919, showing the same high hydrogen-bond occupancies of 96%, and with distances 3.10 Å and 3.08 Å in our MD results, respectively. The CO motifs of the amide group of ligands **1** and **2** form hydrogen bond interactions with backbone of Asp1046, showing high hydrogen-bond occupancies of 99% and 98%, and with distances 2.91 Å and 2.96 Å in our MD results, respectively. In addition, there is a H-bond interaction in lower occupancy percentages: the Glu 885, which can forms hydrogen bond interaction with the NH motifs of the amide group of ligands **1** and **2**, with their distances 3.02 Å and 2.96 Å, and with 24.9% and 39.7% occupancy percentages in our MD results, respectively, that contribute more favorablely and less unfavorablely to ligand **2** than to ligand **1**. A similar hydrogen bond pattern is also observed in **1**-VEGFR-2(inactive), **3**-VEGFR-2(active) and **3**-VEGFR-2(inactive) systems.

Table 2

Hydrogen Bonds analysis from MD

system	Donor	acceptor	Distance (Å) [a]	Angle(°) [b]	Occupancy (%)[c]
	Asp1046 NH	Ligand O4	2.91 (0.14)	19.88 (10.06)	99.67
1-VEGFR-2(active)	Cys919 NH	Ligand N1	3.10 (0.14)	25.38 (13.52)	96.56
	Ligand NH	Glu885 OE2	3.02 (0.19)	37.89 (13.11)	24.90
	Asp1046 NH	Ligand O4	3.01 (0.18)	25.53 (11.38)	93.02
1-VEGFR-2(inactive)	Cys919 NH	Ligand N1	3.09 (0.14)	29.73 (14.00)	92.50
	Ligand NH	Glu885 OE2	3.02 (0.18)	21.04 (11.98)	49.34
	Asp1046 NH	Ligand O4	2.96 (0.15)	25.51 (11.18)	98.64
2-VEGFR-2(inactive)	Cys919 NH	Ligand N1	3.08 (0.14)	24.57 (13.27)	96.65
	Ligand NH	Glu885 OE2	2.96 (0.16)	25.22 (11.64)	39.70
	Cys919 NH	Ligand N1	3.08 (0.14)	26.03 (13.55)	96.59
3-VEGFR-2(active)	Asp1046 NH	Ligand O4	3.03 (0.18)	23.97 (11.88)	72.03
	Ligand NH	Glu885 OE2	3.10 (0.19)	32.66 (14.27)	12.17
	Cys919 NH	Ligand N1	3.06 (0.13)	23.02 (13.12)	97.78
3-VEGFR-2(inactive)	Asp1046 NH	Ligand O4	3.01 (0.18)	23.02 (13.12)	83.93
	Ligand NH	Glu885 OE2	3.14 (0.19)	36.31 (13.87)	14.60

[a]The average distance with standard error (SE =standard deviation/$N^{1/2}$) in parentheses between hydrogen-acceptor atom and hydrogen-donor atom in the investigated time period. [b]The average angle with standard error (SE = standard deviation/$N^{1/2}$) in parentheses for hydrogen bond in the investigated time period. [c]Occupancy is in unit of percentage of the investigated time period.

3.2. Binding Free Energy Analysis

The binding free energies of all complexes except **3**-VEGFR-2(active) were calculated by using MM-PB/GBSA program in AMBER. It needs to be noted that the binding free energies calculated with MM-PBSA and MM-GBSA do not reproduce the absolute experimental values accurately, but they have been shown to correlate with the experiment values well. Given the more underestimation of MM-GBSA calculation, compared with that of MM-PBSA, our discussion about binding free energy is mainly based on the results of MM-PBSA. In Table 3, we present the predicted and experimental relative binding free energies, together with their respective enthalpic and entropic contributions. The experimental binding free energy values (ΔG_{exp}) derived from IC_{50} values are -12.66 and -12.79 kcal/mol for the complexes of **1**-VEGFR-2(active) and **2**-VEGFR-2(inactive). As can been seen, MM-PBSA calculations verified that ligands **1** and **2** have almost the same activities against VEGFR-2 ($\Delta G_{\mathbf{1}\text{-VEGFR-2(active)}}$ = -26.68 kcal/mol, $\Delta G_{\mathbf{2}\text{-VEGFR-2(inactive)}}$ = -27.47 kcal/mol, $\Delta\Delta G$=0.79 kcal/mol), in good agreement with the experimental data. In addition, the free energy calculations show that ligand **1** binding to active conformation is 4.51 kcal /mol more stable than binding to inactive conformation, which is in agree with the experimental observation that ligand **1** binds to and stabilizes the

DFG-in conformation. In addition, the binding free energy of compound **3** binding to inactive conformation using the MM-PBSA method is very high (ΔG = -19.96 kcal/mol), which is in agree with the experimental observation that ligand **3** exhibits drastically diminished potency.

Besides ranking the binding free energies correctly, another advantage of MM-PBSA and MM-GBSA is that it allows us to decompose the total binding free energy into individual components, thereby enabling us to understand the complex binding process in detail. According to the energy components of the binding free energies, the major favorable contributors to ligand binding are vdW and electrostatic terms, whereas polar solvation ($\Delta G_{ele,sol}$) and entropy terms oppose binding. The van der Waals interactions and the nonpolar salvation energies responsible for the burial of inhibitor's hydrophobic groups upon binding are the basis for favorable binding free energies. The binding pocket is primarily hydrophobic, which is suggested by MM-PBSA and MM-GBSA calculations (Table 3), where the absolute value of the ΔG_{vdW} term (-58.23 kcal/mol for **1**-VEGFR-2(active), -58.64 kcal/mol for **1**-VEGFR-2(inactive), -64.62 kcal/mol for **2**-VEGFR-2(inactive) , -57.89 kcal/mol for **3**-VEGFR-2(inactive)) is greater than that of the ΔG_{ele} term (-25.02 kcal/mol for **1**-VEGFR-2(active), -21.62 kcal/mol for **1**-VEGFR-2(inactive), -24.73 kcal/mol for **2**-VEGFR-2(inactive) , -17.26 kcal/mol for **3**-VEGFR-2(inactive)). The favorable Coulomb interactions within the protein-inhibitor complexes are counteracted by the unfavorable electrostatics of desolvation upon binding. Consequently, the total electrostatic interaction contributions are unfavorable to binding in all systems. If we examine the contributions to each binding energy, the most important term which dictates the difference in the binding affinity is ΔE_{vdW}. The binding of ligand **2** to inactive conformation of VEGFR-2 gains over 5.98 kcal/mol and 6.73 kcal/mol of ΔE_{vdW} value compared with ligands **1** and **3** binding to inactive conformation, respectively, which can be explained by the more extensive hydrophobic interactions it can make in the VEGFR-2 back-pocket generated upon induced movement of the activation loop by virtue of its additional 4-Cl-phenyl substituent.

Table 3

MM-PBSA and MM-GBSA binding free energies and its components for the studied complexes for the last 10 ns MD trajectories[a]

	1-VEGFR-2(active)	**1**-VEGFR-2(inactive)	**2**-VEGFR-2(inactive)	**3**-VEGFR-2(inactive)
ΔG_{vdW}	-58.23 (0.08)	-58.64 (0.08)	-64.62 (0.08)	-57.89(0.08)
ΔG_{ele}	-25.02 (0.10)	-21.62 (0.10)	-24.73 (0.10)	-17.26(0.14)
ΔG_{MM}	-83.24 (0.12)	-80.26 (0.11)	-89.35 (0.11)	-75.14(0.15)
$\Delta G_{ele,sol}$(GB)	35.38 (0.07)	33.29 (0.06)	35.19(0.06)	32.24(0.09)
$\Delta G_{np,sol}$(GB)	-7.35 (0.01)	-7.00 (0.01)	-7.89 (0.01)	-7.36(0.01)

ΔG_{sol} (GB)	28.03 (0.07)	26.40 (0.06)	27.30 (0.06)	24.88(0.09)
$\Delta G_{ele,sol}$(PB)	45.64 (0.09)	40.00 (0.07)	45.30 (0.08)	41.06(0.12)
$\Delta G_{np,sol}$(PB)	-4.48 (0.00)	-4.38 (0.00)	-5.12(0.00)	-4.87(0.00)
ΔG_{sol}(PB)	41.16 (0.09)	35.61 (0.07)	40.18 (0.08)	36.19(0.12)
ΔH(GB)	-55.21 (0.09)	-53.86 (0.09)	-62.05 (0.10)	-50.26(0.10)
ΔH(PB)	-42.08 (0.10)	-44.64 (0.10)	-49.17 (0.10)	-38.96(0.12)
TΔS	-15.41 (2.57)	-22.47 (1.83)	-21.70 (2.26)	-19.00(2.38)
ΔG_{pred}(GB)	-39.80	-31.39	-40.36	-31.26
ΔG_{pred} (PB)	-26.68	-22.17	-27.47	-19.96
IC_{50}(nM)[b]	0.60nM	-	0.48nM	1500 nM
ΔG_{exp}	-12.66	-	-12.79	-8.00

[a]Mean energies are in kcal/mol, with corresponding standard errors (SE = standard deviation/$N^{1/2}$) in parentheses. ΔH: the enthalpy changes, $\Delta H = \Delta G_{ele} + \Delta G_{vdW} + \Delta G_{np,sol} + \Delta G_{ele,sol}$. T$\Delta$S: the entropy changes. ΔG_{pred}: the calculated binding free energy by MM-PB(GB)SA method. ΔG_{exp}: the experimental binding free energy calculated according to the IC_{50} by $\Delta G \approx -RT \ln IC_{50}$.[b] ref.[16,17]

3.3. Binding Free Energy Decomposition

To identify the key residues related with the binding process, the binding free energy between the protein and inhibitor was decomposed into the contribution of each residue using MM-GBSA approach. In the present work, it was considered as a hot spot if any residue contributes more than 1.0 kcal/mol to the binding free energy of the complex. The interaction information in all complexes is shown in Fig. 5. The contributions of key residues for all complexes are compared in Fig. 6. As can be seen from Fig. 5 and 6, the major favorable energy contributions originate predominantly from the residues Leu840, Val848, Ala866, Lys868, Leu889, Val899, Thr916, Phe918, Cys919, Leu1035, Cys1045, Asp1046, and Phe1047 of VEGFR-2 in common in all complexes. It is interesting that almost all those important residues are hydrophobic, involved in the lipophilic pocket by Phe1047 of DFG-out loop, which can form strong van der Waals interactions with the inhibitors.

4. Conclusions

In this study, MD simulations and binding free energy calculations were performed to investigate the structural mechanisms of inhibitors binding to active and inactive conformations of VEGFR-2, respectively. We find that the active conformation binding to Type-I inhibitor appears somewhat more flexible when compared to the unbound form. In contrast, the binding of Type II inhibitor **2** to the inactive conformation helps to stabilize the inactive conformation of the protein. Calculations of binding free energy verify that inhibitors **1** and **2** have almost the same activities against VEGFR-2. In addition, binding free energy calculations suggest that ligand **1**

binds to and stabilizes the DFG-in conformation of VEGFR-2, which is in agree with the experimental observation. Molecular dynamics simulations and binding free energy calculations of **3** binding to VEGFR-2 can give a good explanation of the drastically diminished potency. The decomposition of binding free energy into each interaction type suggests that van der Waals interactions provided the substantial driving force for the binding process. The important hydrophobic property of the terminal 4-Cl phenyl was required to be type II inhibitors. The per-residue energy decomposition demonstrates the most favorable contribution came from Leu840, Val848, Ala866, Lys868, Leu889, Val899, Thr916, Phe918, Cys919, Leu1035, Cys1045, Asp1046, and Phe1047. The findings in this work could provide a better structural understanding of type I and type II inhibitors targeting the DFG-in and DFG-out form of protein kinase and a basis for further rational design of new inhibitors against VEGFR-2.

Conflicts of interest

The authors declare that they have no conflicts of interest.

Acknowledgement

The authors are gratefully acknowledged financial support from the National Science Foundation of China (No.81202413) and Science and Technology Planning Project of Guangdong Province, China (No.2011B050200006). The calculations of the ligands were performed in the China ScGrid of Supercomputing Center of Chinese Academy of Science.

References

1. G.D. Yancopoulos, S. Davis, N.W. Gale, J.S. Rudge, S.J. Wiegand, J. Holash, Vascular-specific growth factors and blood vessel formation. Nature 407 (2000) 242–248
2. G.D Hartman, M.E Fraley., M.T. Bilodeau, Kinase insert domain-containing receptor kinase inhibitors as anti-angiogenic agents. Expert Opin. Investig. Drugs 11 (2002) 737–745
3. J. Folkman, Anti-angiogenesis: new concept for therapy of solid tumors. Ann. Surg.175 (1972) 409–416.
4. L.A. Liotta, P.S Steeg., W.G. Stetler-Stevenson, Cancer metastasis and angiogenesis: an imbalance of positive and negative regulation. Cell 64 (1991) 327–336
5. D.J. Hicklin, L.M. Ellis, Role of the vascular endothelial growth factor pathway in tumor growth and angiogenesis. J. Clin. Oncol. 23 (2005) 1011–1027

6. N. Ferrara, Vascular endothelial growth factor: basic science and clinical progress. Endocr. Rev. 25 (2004) 581–611

7. P. Carmeliet, V. Ferreira, G. Breier, S. Pollefeyt, L. Kieckens, M. Gertsenstein, M. Fahrig, A. Vandenhoeck, K. Harpal, C. Eberhardt, C. Declercq, J. Pawling, L. Moons, D. Collen, W. Risau, A. Nagy Abnormal blood vessel development and lethality in embryos lacking a single VEGF allele. Nature 380 (1996) 435–439

8. N. Ferrara, T. Davis–Smyth, The biology of vascular endothelial growth factor. Endocr. Rev. 18 (1997) 4–25

9. K. Holmes, O. L. Roberts, A.M. Thomas, M.J. Cross, Vascular endothelial growth factor receptor-2: structure, function, intracellular signaling and therapeutic inhibition. Cell Signal. 19 (2007) 2003–2012

10. M.A. Bogoyevitch, D. Fairlie, A new paradigm for protein kinase inhibition: blocking phosphorylation without directly targeting ATP binding. Drug Discov. Today 12 (2007) 622–633

11. Y. Liu, N.S. Gray, Rational design of inhibitors that bind to inactive kinase conformations. Nat. Chem. Biol. 2 (2006) 358–364

12. L. Garuti, M. Roberti, G. Bottegoni, Non-ATP competitive protein kinase inhibitors. Curr. Med. Chem. 17 (2010) 2804–2821

13. B. Okram, A. Nagle, F.J. Adrian, C. Lee, P. Ren, X. Wang, T. Sim, Y. Xie, X. Wang, G. Xia, G. Spraggon, M. Warmuth, Y. Liu, N.S. Gray, A general strategy for creating “inactive-conformation” Abl inhibitors. Chem. Biol. 13 (2006) 779–786

14. L.O. Kirkland, C. McInnes , Non-ATP competitive protein kinase inhibitors as anti-tumor therapeutics. Biochem. Pharmacol. 77 (2009) 1561–1571

15. A. Kiselyov, K.V. Balakin, S.E. Tkachenko, N.P. Savchuk, Recent progress in development of non-ATP competitive small-molecule inhibitors of protein kinesis. Mini Rev. Med .Chem.6 (2006) 711–717

16. J.C. Harmange, M.M. Weiss, J. Germain, A.J. Polverino, G. Borg, J. Bready, D. Chen, D. Choquette, A. Coxon, T. DeMelfi, L. DiPietro, N. Doerr, J. Estrada, J. Flynn, R.F. Graceffa, S.P. Harriman, S. Kaufman, D.S. La, A. Long, M.W. Martin, S. Neervannan, V.F. Patel, M. Potashman, K. Regal, P.M. Roveto, M.L. Schrag, C. Starnes, A. Tasker, Y. Teffera, L. Wang, R.D. White, D.A. Whittington , R. Zanon, Naphthamides as novel and potent vascular endothelial growth factor receptor tyrosine kinase inhibitors: design, synthesis, and evaluation. J. Med. Chem. 51 (2008)1649-1667

17. M.M. Weiss, J.C. Harmange, A.J. Polverino, D. Bauer, L. Berry, V. Berry, G. Borg, J. Bready, D. Chen, D. Choquette, A. Coxon, T. DeMelfi, N. Doerr, J. Estrada, J. Flynn, R.F. Graceffa, S.P. Harriman, S. Kaufman, D.S. La, A. Long, S. Neervannan, V.F. Patel, M. Potashman, K. Regal, P.M. Roveto, M.L. Schrag, C. Starnes, A. Tasker, Y. Teffera, D.A. Whittington, R. Zanon , Evaluation of a series of naphthamides as potent, orally active vascular endothelial growth factor receptor-2 tyrosine kinase inhibitors. J. Med. Chem. 51 (2008) 1668-1680

18. K. Arnold, L. Bordoli, J. Kopp, T. Schwede, The SWISS-MODEL Workspace: A web-based environment for protein structure homology modelling. Bioinformatics 22 (2006) 195-201

19. P. Benkert, M. Biasini, T. Schwede, Toward the estimation of the absolute quality of individual protein structure models. Bioinformatics 27(2011)343–350

20. Sybyl 7.3, T.I., 1699 South Hanley Rd., St. Louis, MI 63144, USA

21. M. Frisch, G. Trucks, H. Schlegel, G. Scuseria, M. Robb, J. Cheeseman, J. Montgomery Jr, T. Vreven, K. Kudin, J. Burant. Gaussian 03; Gaussian, Inc.: Wallingford, CT, 2004

22. C.I. Bayly, P. Cieplak, W. Cornell , P.A. Kollman, A well behaved electrostatic potential based method using charge restraints for deriving atomic charges: the RESP model. J. Phys. Chem. 97(1993) 10269−10280

23. J. Wang, W. Wang, P. A. Kollman, D.A. Case, Automatic atom type and bond type perception in molecular mechanical calculations. J. Mol. Graph. Model. 25 (2006) 247−260

24. J. Wang, R.M. Wolf, J.W. Caldwell, P.A. Kollman, D.A. Case, Development and testing of a general amber force field. J. Comput. Chem. 25 (2004) 1157−1174

25. V. Hornak, R. Abel, A. Okur, B. Strockbine, A. Roitberg, C. Simmerling, Comparison of multiple Amber force fields anddevelopment of improved protein backbone parameters. Proteins: Struct., Funct., Bioinf. 65 (2006) 712−725

26. W.L. Jorgensen , J. Chandrasekhar, J.D. Madura, R.W. Impey, M.L. Klein, Comparison of simple potential functions for simulating liquid water. J. Chem. Phys. 79 (1983) 926−935

27. D.A. Case, T.A. Darden, T.E. Cheatham III, C.L. Simmerling, J. Wang, R.E. Duke, R. Luo, R.C. Walker, W. Zhang, K.M. Merz, B. Roberts, S. Hayik, A. Roitberg, G. Seabra, J. Swails, A.W. Goetz, I. Kolossváry, K.F. Wong, F. Paesani, J. Vanicek, R.M. Wolf, J. Liu, X. Wu, S.R. Brozell, T. Steinbrecher, H. Gohlke, Q. Cai, X. Ye, J. Wang, M.J. Hsieh, G. Cui, D.R. Roe, D.H. Mathews, M.G. Seetin, R. Salomon-Ferrer, C. Sagui, V.

Babin, T. Luchko, S. Gusarov, A. Kovalenko, P.A. Kollman, AMBER 12, 2012, University of California, San Francisco

28. R. Salomon-Ferrer, A.W. Götz, D. Poole, S. Le Grand, R.C. Walker, Routine microsecond molecular dynamics simulations with AMBER on GPUs. 2. Explicit Solvent Particle Mesh Ewald. J. Chem. Theory Comput .9 (2013) 3878-3888
29. T. Darden, D. York, L. Pedersen, Particle mesh Ewald: An N·log-(N) method for Ewald sums in large systems. J. Chem. Phys. 98 (1993) 10089−10092
30. J.P. Ryckaert, G. Ciccotti, H.J.C. Berendsen, Numerical integration of the cartesian equations of motion of a system with constraints: molecular dynamics of n-alkanes. J. Comput. Phys. 23 (1977) 327−341
31. P.A. Kollman, I. Massova, C. Reyes, B. Kuhn, S. Huo, L. Chong, M. Lee, T. Lee, Y. Duan, W. Wang, O. Donini, P. Cieplak, J. Srinivasan, D.A. Case, T.E. Cheatham, Calculating structures and free energies of complex molecules: combining molecular mechanics and continuum models. Acc. Chem. Res. 33 (2000) 889–897
32. W. Rocchia, E. Alexov, B. Honig, Extending the applicability of the nonlinear Poisson-Boltzmann equation: Multiple dielectric constants and multivalent ions. J. Phys. Chem. B 105 (2001) 6507–6514
33. A. Onufriev, D. Bashford, D.A. Case, Exploring protein nativestates and large-scale conformational changes with a modified generalized born model. Proteins: Struct., Funct., Bioinform. 55 (2004) 383–394
34. S.T. Wlodek, T.W. Clark, L.R. Scott, J.A. McCammon, Molecular dynamics of acetylcholinesterase dimer complexed with tacrine. J. Am. Chem. Soc. 119 (1997) 9513–9522

Fig. 1. The structures and IC_{50} values of compounds **1**-**3**

Fig.2. (a) X-ray structural comparison between **1** binding to active conformation (green) and **2** binding to inactive conformation (cyan) of VEGFR-2. Structural comparison between initial (green) and MD simulated representative snapshots (cyan) of (b) **1**-VEGFR-2(active), (c) **1**-VEGFR-2(inactive), (d) **2**-VEGFR-2(inactive), (e) **3**-VEGFR-2(active), (f) **3**-VEGFR-2(inactive).Yellow dots represent hydrogen bonds. For clarity, nonpolar hydrogen was omitted. (VEGFR-2 in colored ribbon, ligands in ball and stick model, the key residues in capped sticks model)

Fig. 3. RMSDs of backbone atoms (C, Cα, and N) of the protein, backbone atoms (C, Cα, and N) of binding pocket (residues within 5 Å around each inhibitor), and the heavy atoms in the ligand for (a) **1**-VEGFR-2(active), (b) **1**-VEGFR-2(inactive), (c) **2**-VEGFR-2(inactive), (d) **3**-VEGFR-2(active), and (e) **3**-VEGFR-2(inactive). (f) RMSDs of backbone atoms (C, Cα, and N) of unbound VEGFR-2.

Fig. 4. RMSF of each residue of the active conformation (a) and inactive conformation (b) protein for the complexes obtained from the crystal structure and systems obtained from 80 ns MD simulation.

Fig. 5. Per-residue binding free energy decomposition of: (a) **1**-VEGFR-2(active), (b) **1**-VEGFR-2(inactive), (c) **2**-VEGFR-2(inactive), and (d) **3**-VEGFR-2(inactive).

Fig. 6. Comparison of residues of VEGFR-2 that contribute more than 1.0 kcal/mol to the binding free energy of the complexes.

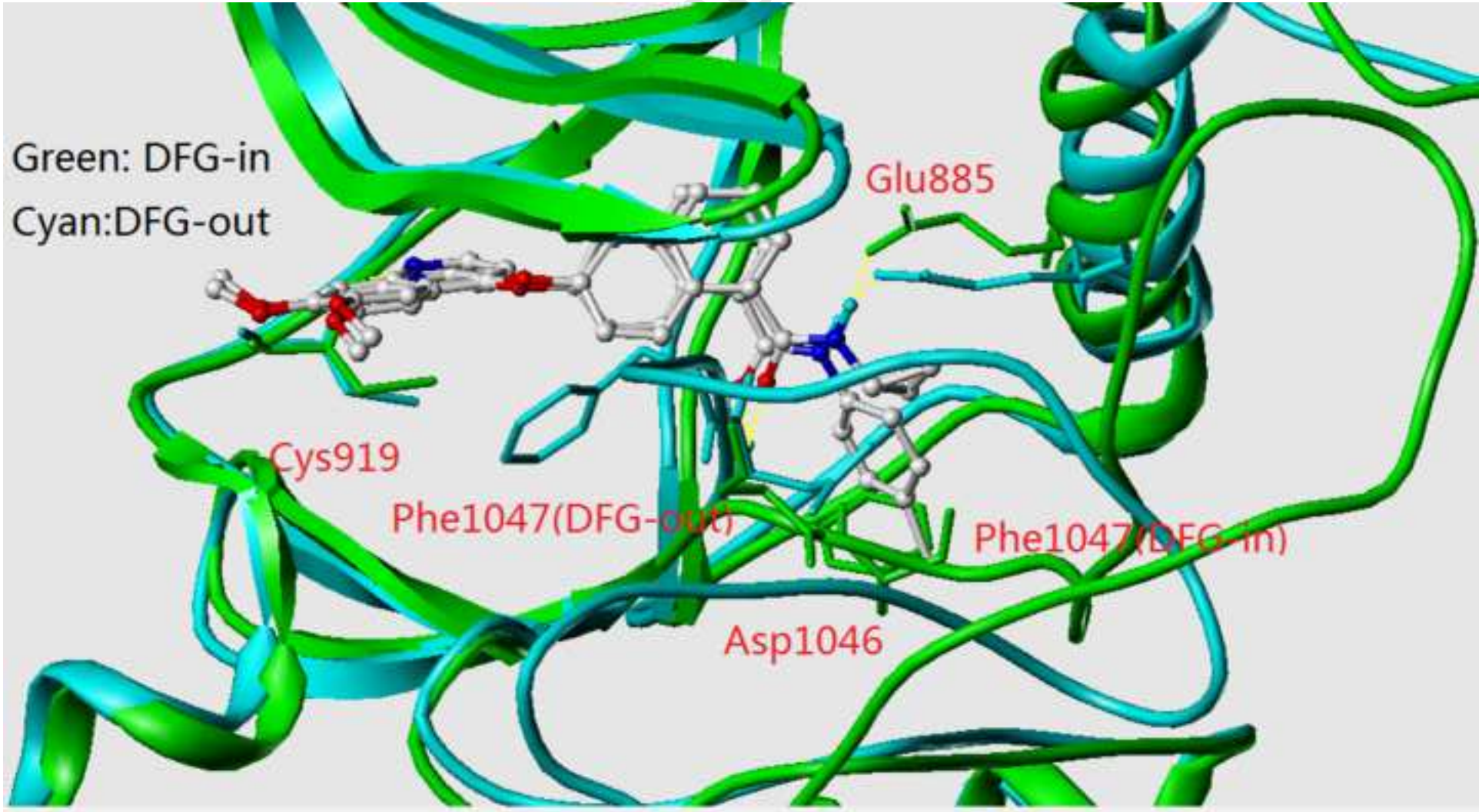
Green: DFG-in
Cyan:DFG-out
Glu885
Cys919
Phe1047(DFG-out)
Phe1047(DFG-in)
Asp1046

Fig 1

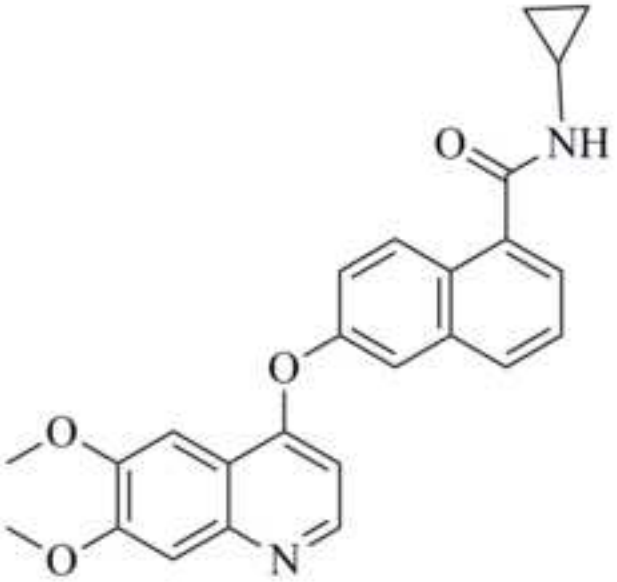

1

IC_{50}=0.6nM

Type I inhibitor

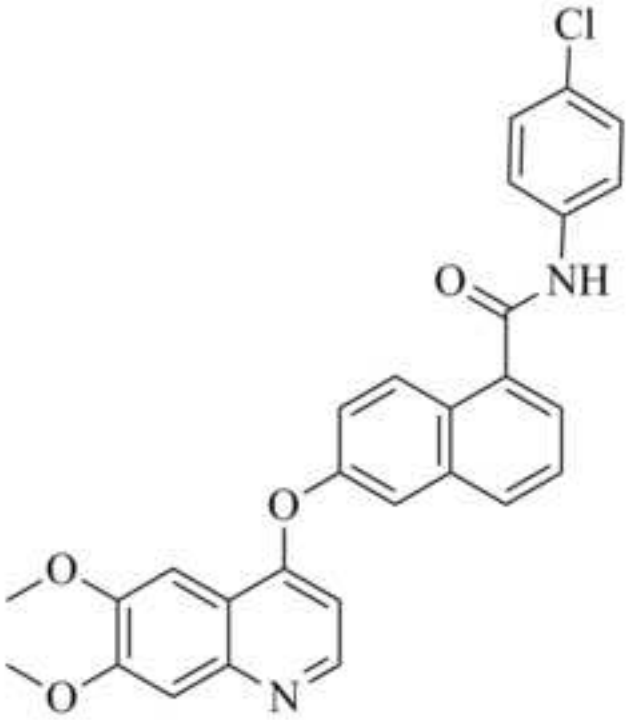

2

IC_{50}=0.48nM

Type II inhibitor

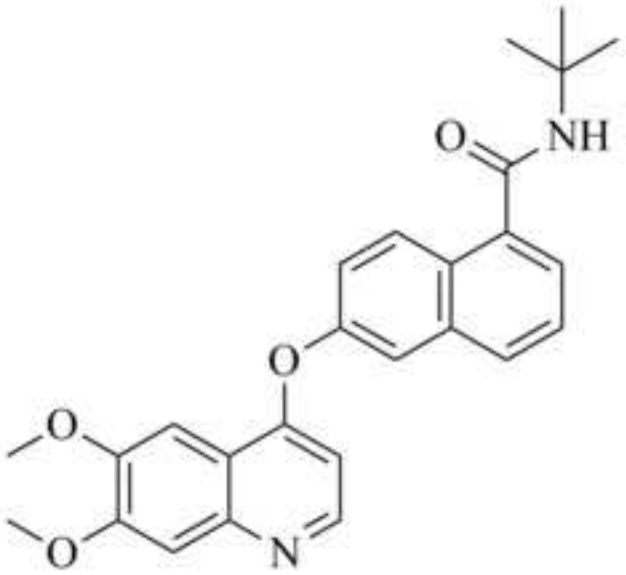

3

IC_{50}=1500nM

Fig 2(a)

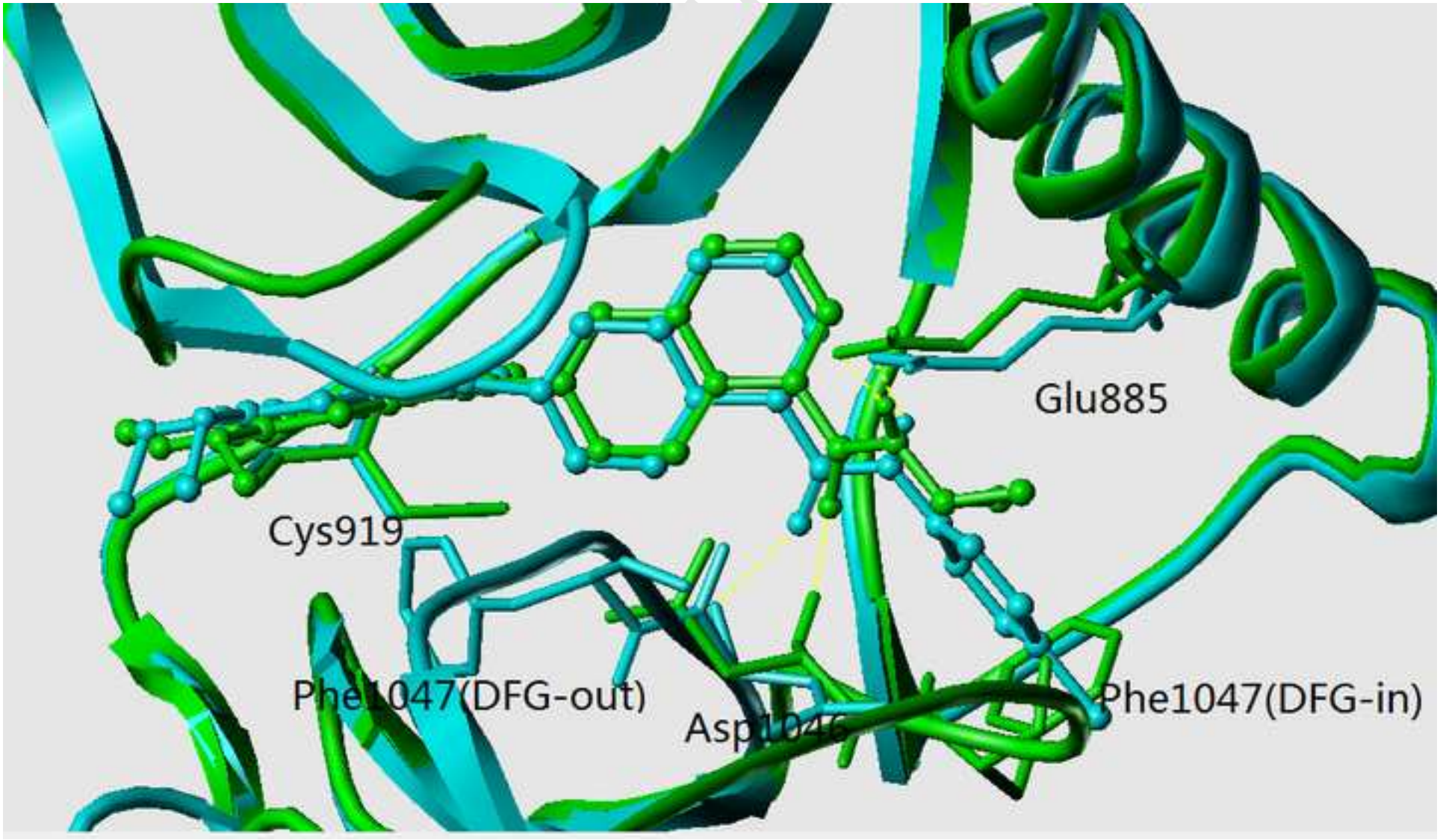

Fig 2(b)

Fig 2(c)

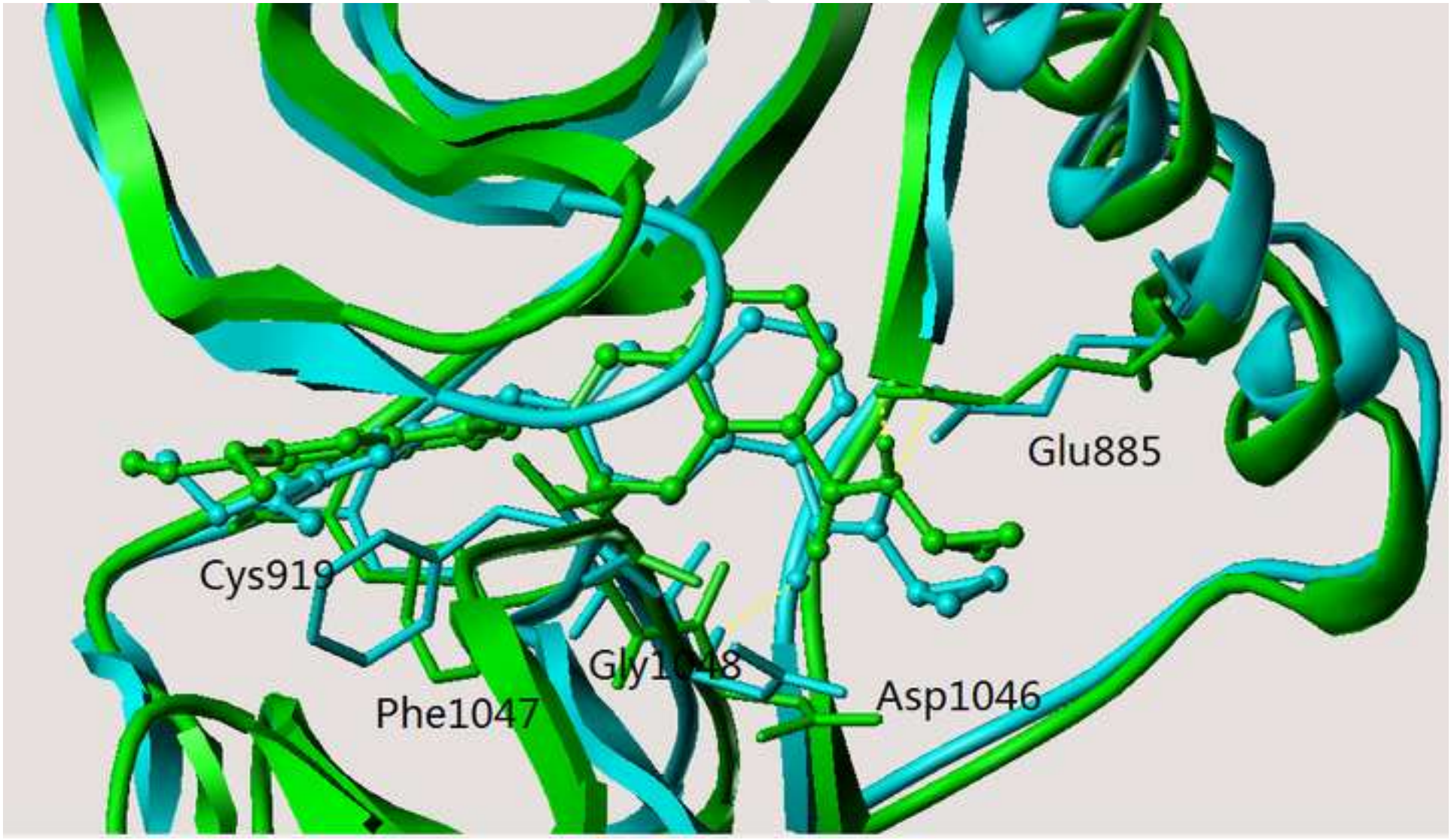

Fig 2(d)

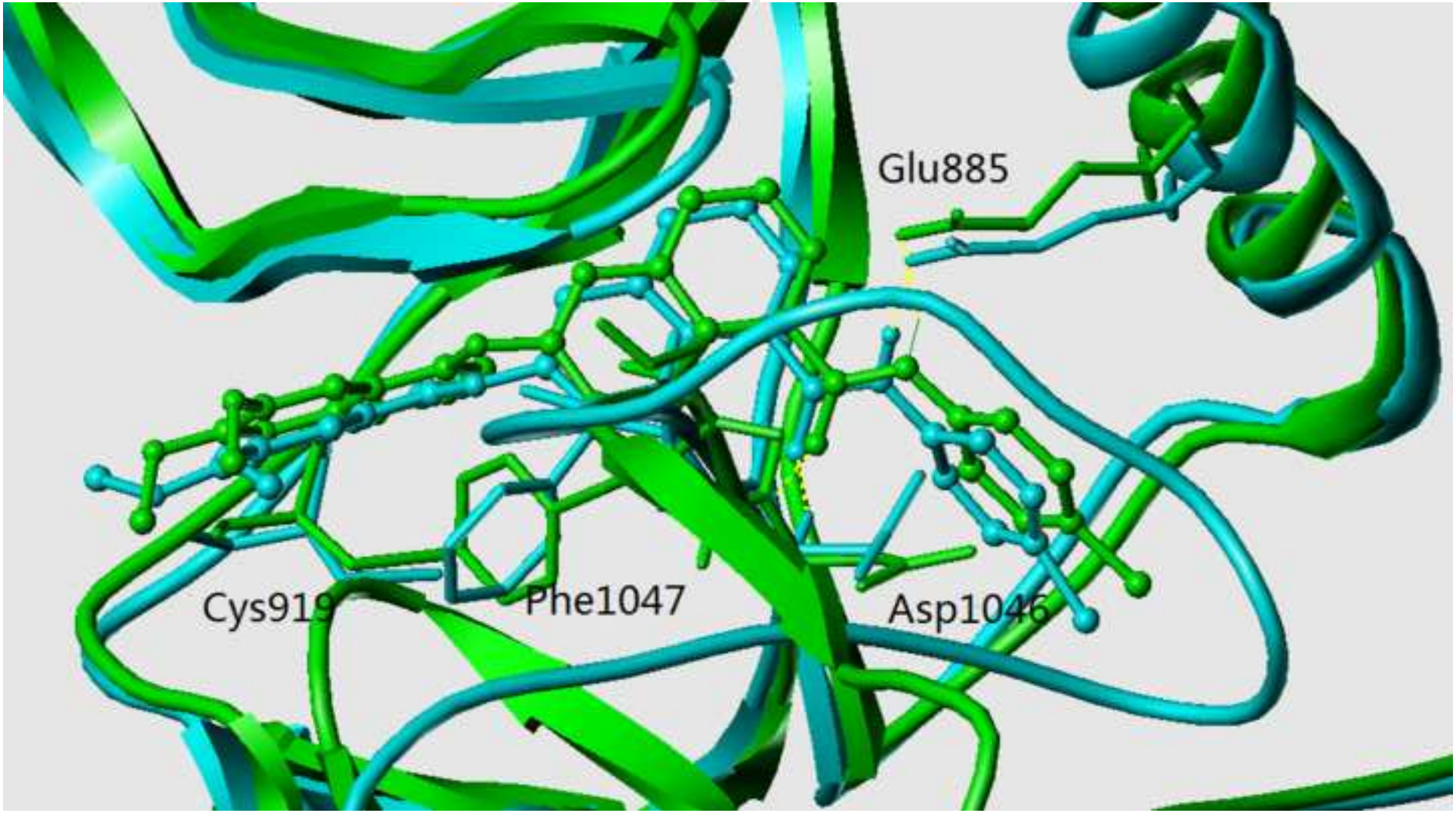

Fig 2(e)

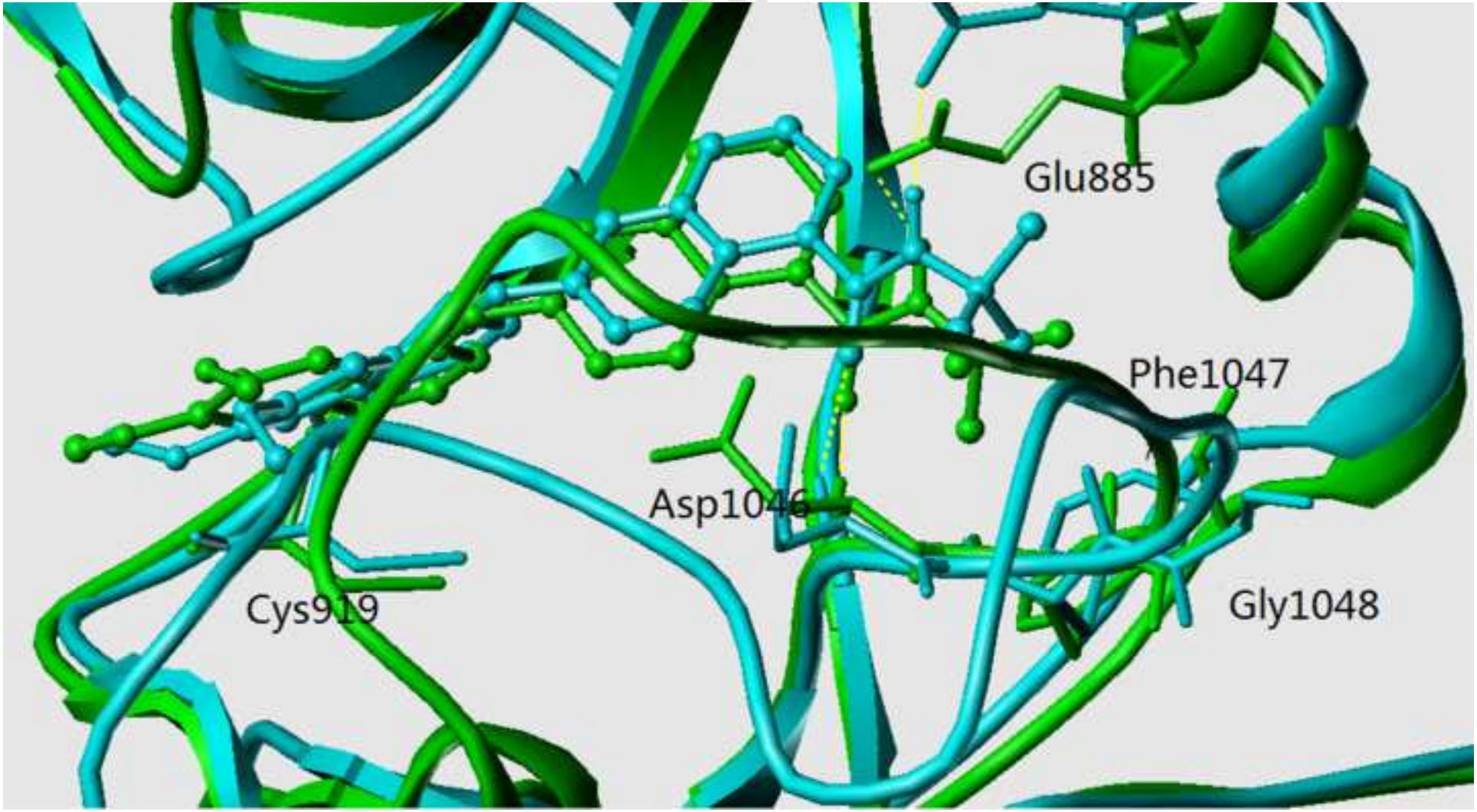

Fig 2(f)

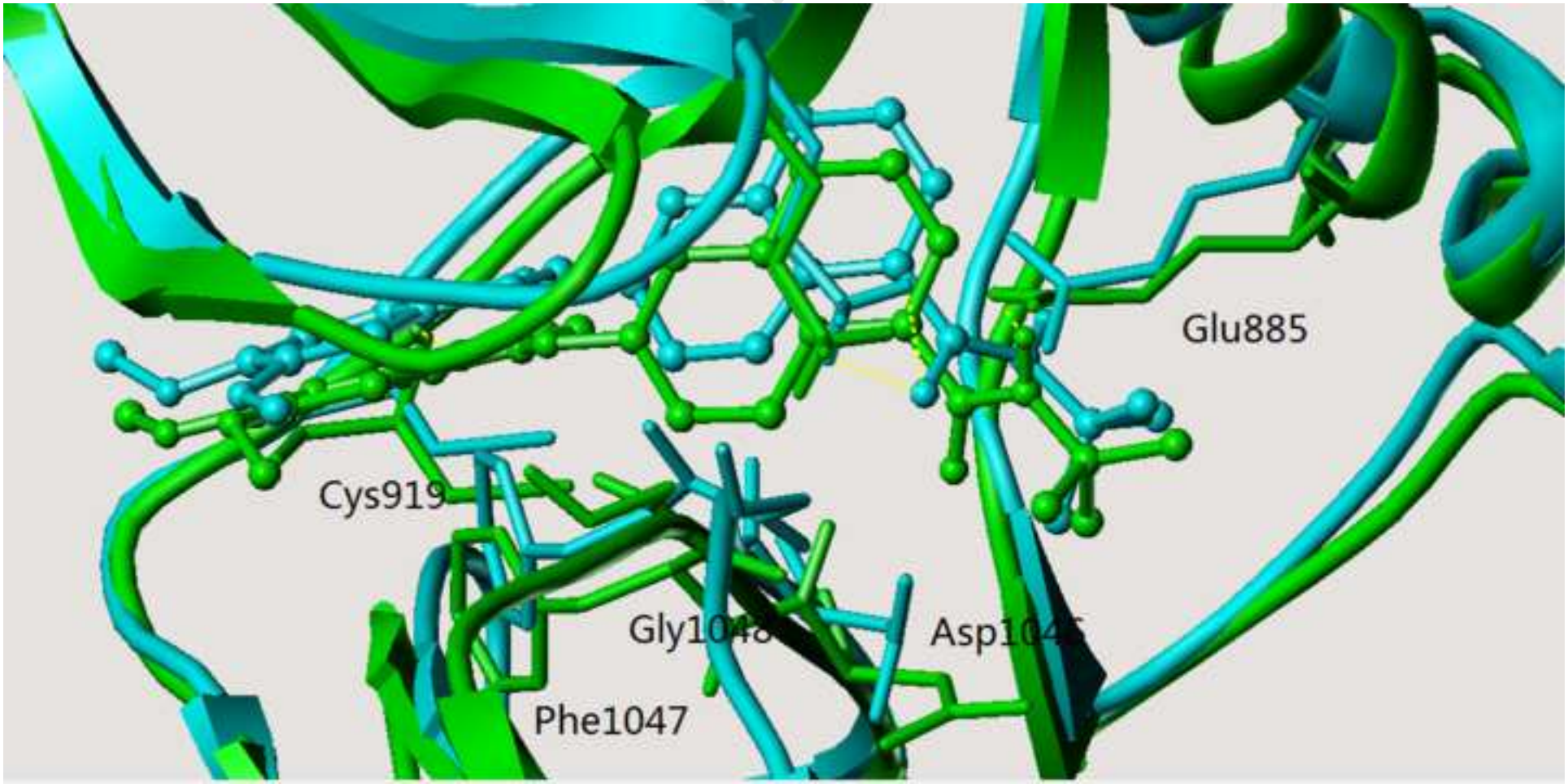

Fig 3(a)

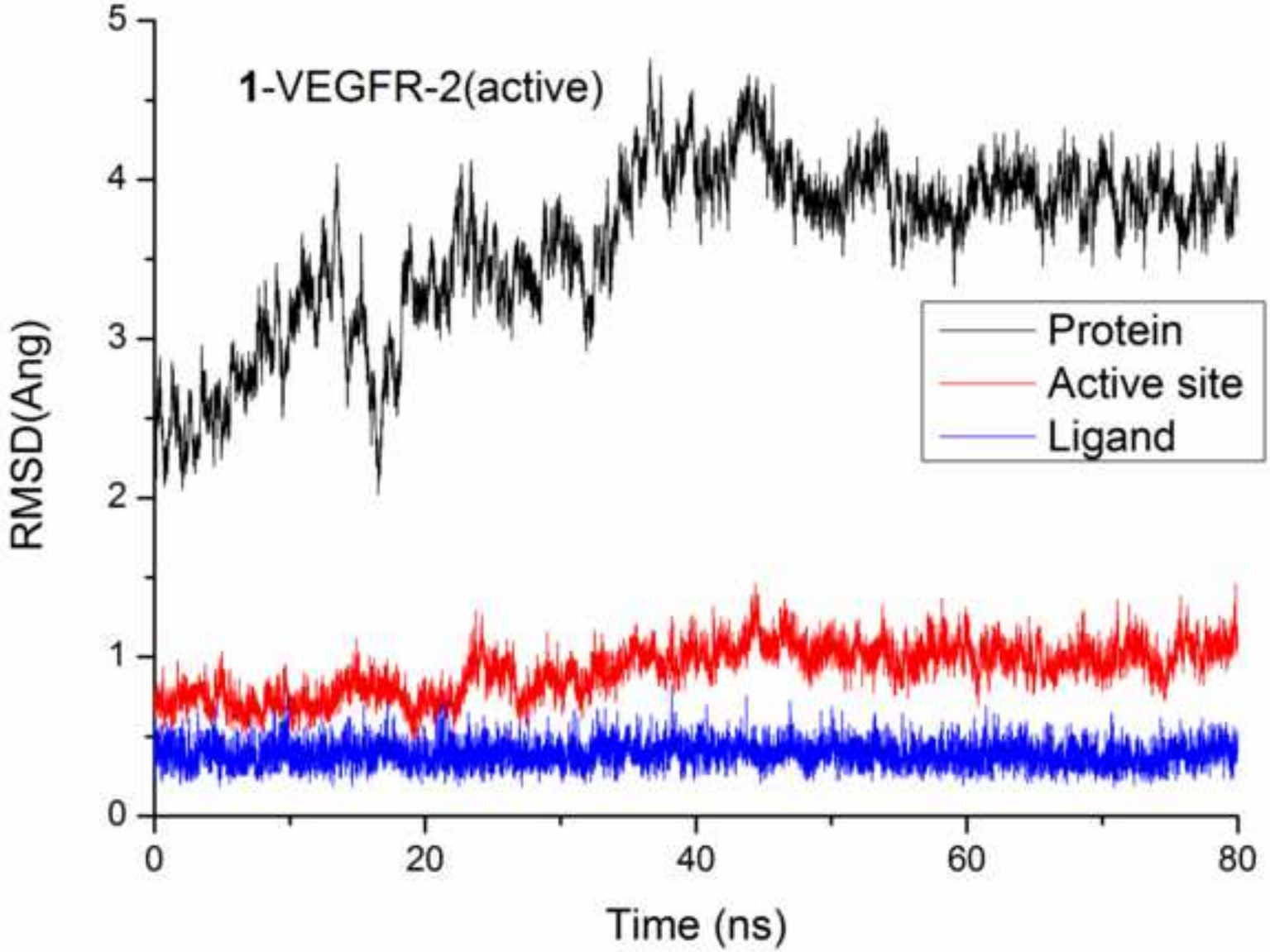
1-VEGFR-2(active)
RMSD(Ang)
Time (ns)
Protein
Active site
Ligand
0
1
2
3
4
5
0
20
40
60
80

Fig 3(b)

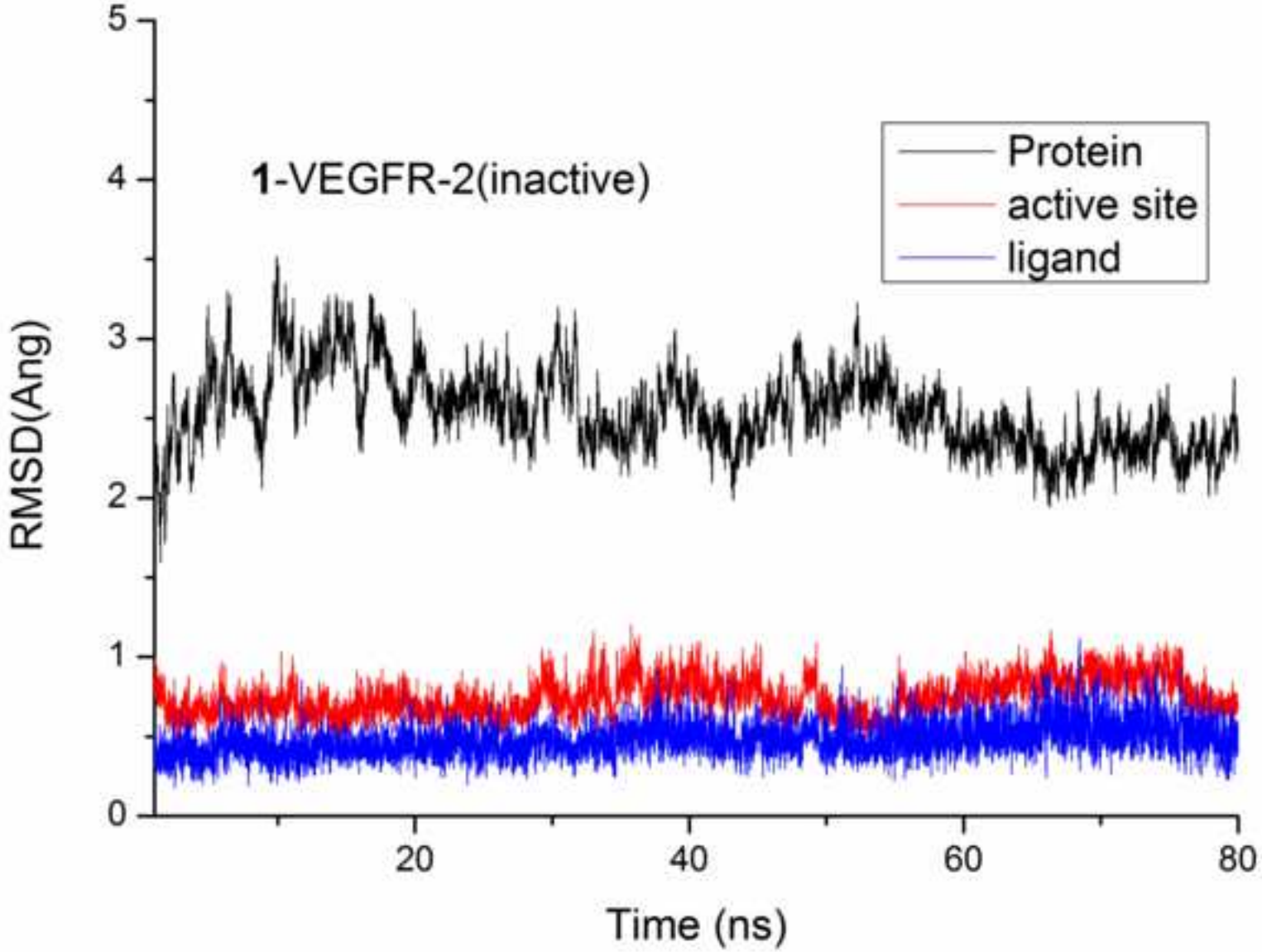
1-VEGFR-2(inactive)
Protein
active site
ligand
RMSD(Ang)
Time (ns)
0
1
2
3
4
5
20
40
60
80

Fig 3(c)

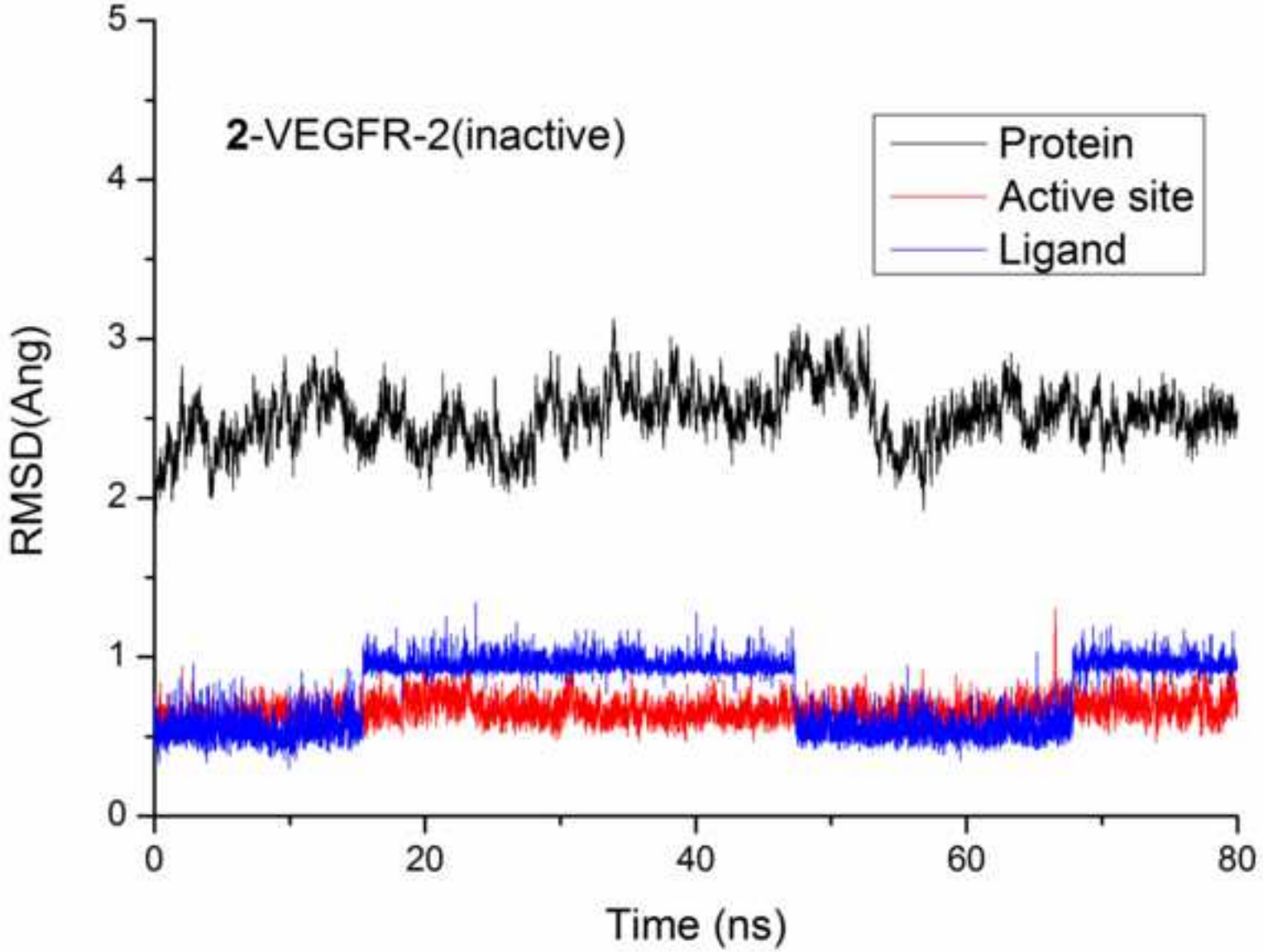
2-VEGFR-2(inactive)
Protein
Active site
Ligand
RMSD(Ang)
Time (ns)
0
1
2
3
4
5
0
20
40
60
80

Fig 3(d)

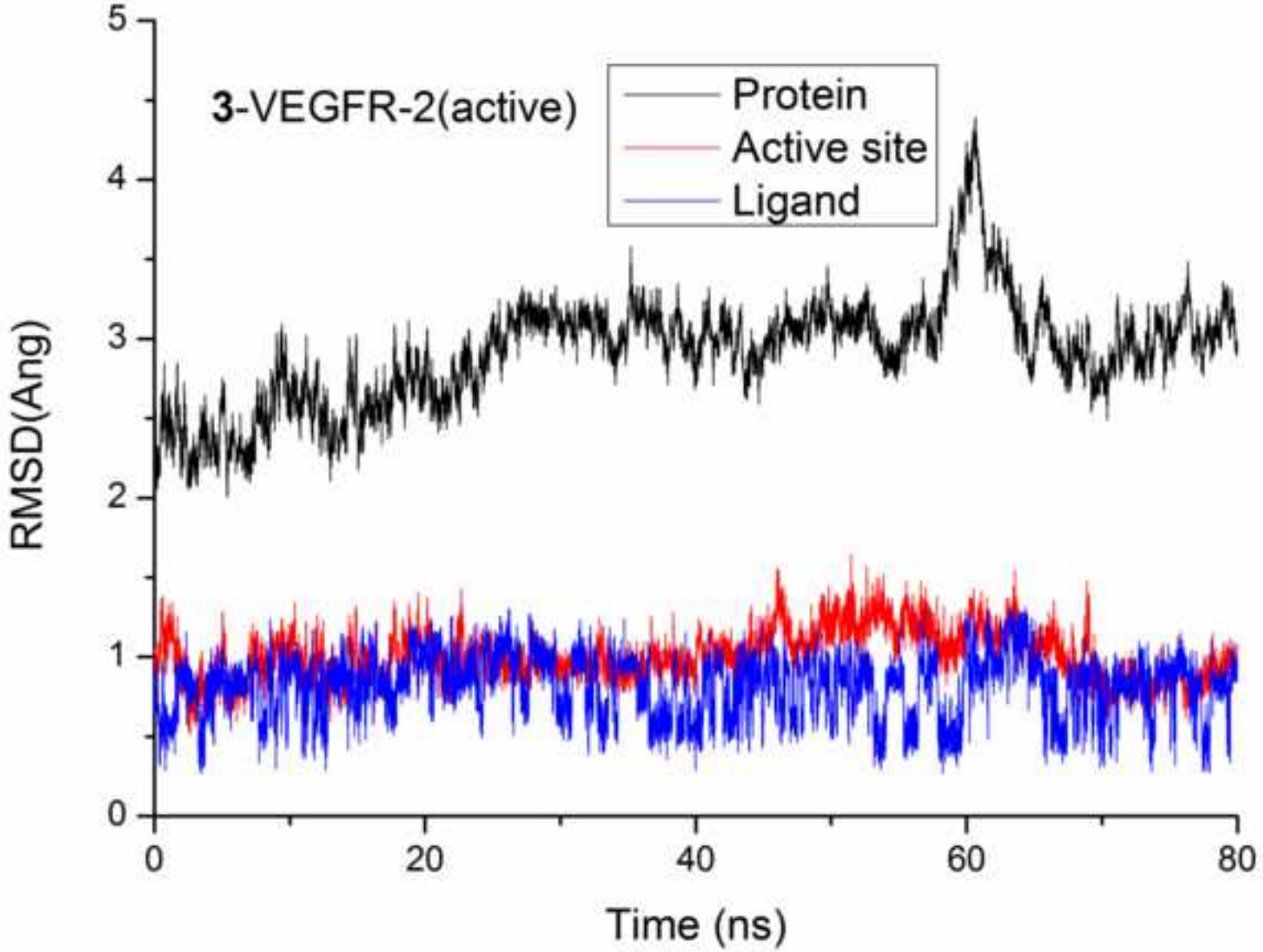
3-VEGFR-2(active)
Protein
Active site
Ligand
RMSD(Ang)
Time (ns)
0
1
2
3
4
5
0
20
40
60
80

Fig 3(e)

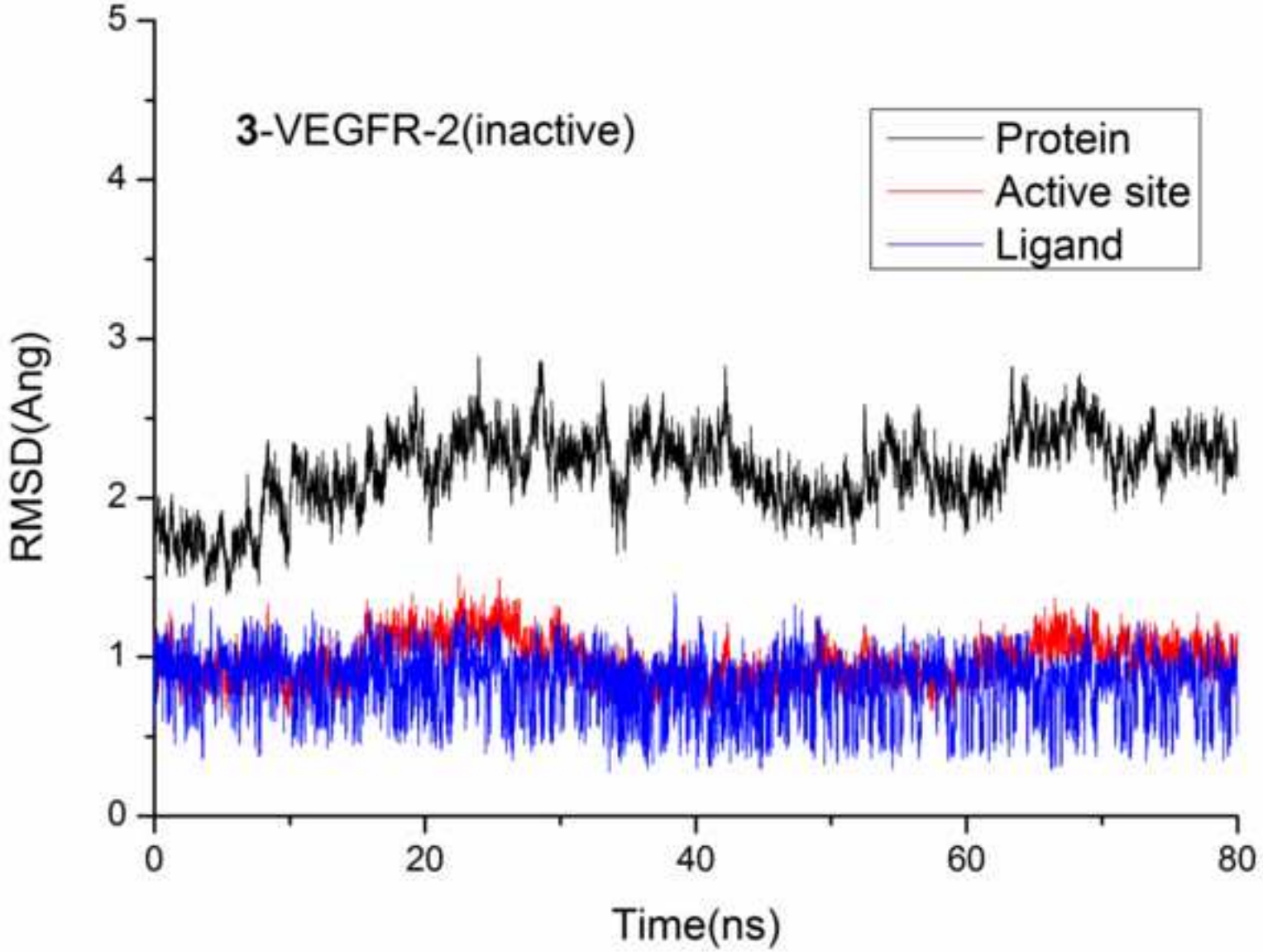
3-VEGFR-2(inactive)
Protein
Active site
Ligand
RMSD(Ang)
Time(ns)
0
1
2
3
4
5
0
20
40
60
80

Fig 3(f)

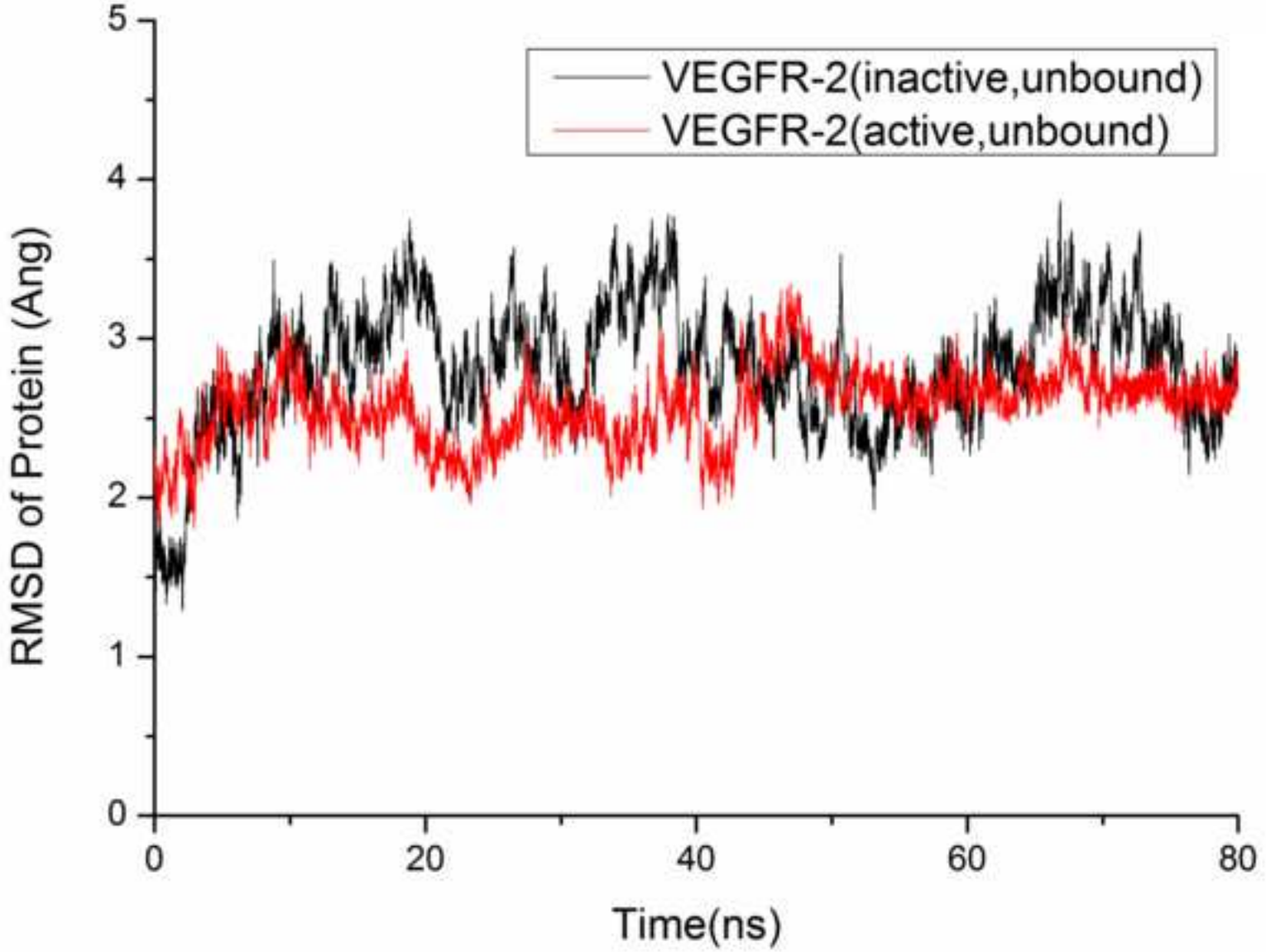
VEGFR-2(inactive,unbound)
VEGFR-2(active,unbound)
RMSD of Protein (Ang)
Time(ns)
0
1
2
3
4
5
0
20
40
60
80

Fig 4(a)

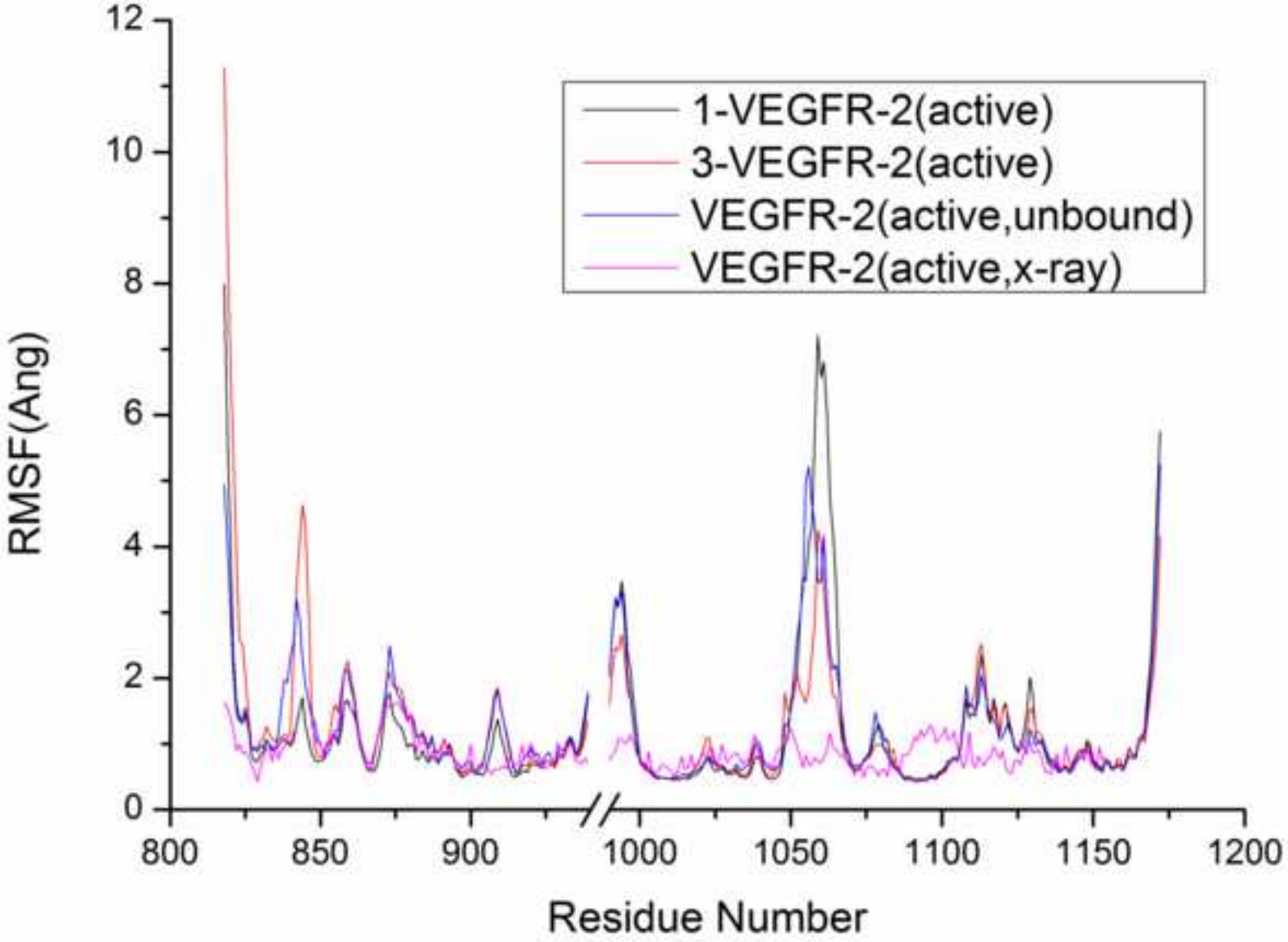
RMSF(Ang)
Residue Number
1-VEGFR-2(active)
3-VEGFR-2(active)
VEGFR-2(active,unbound)
VEGFR-2(active,x-ray)
0
2
4
6
8
10
12
800
850
900
1000
1050
1100
1150
1200

Fig 4(b)

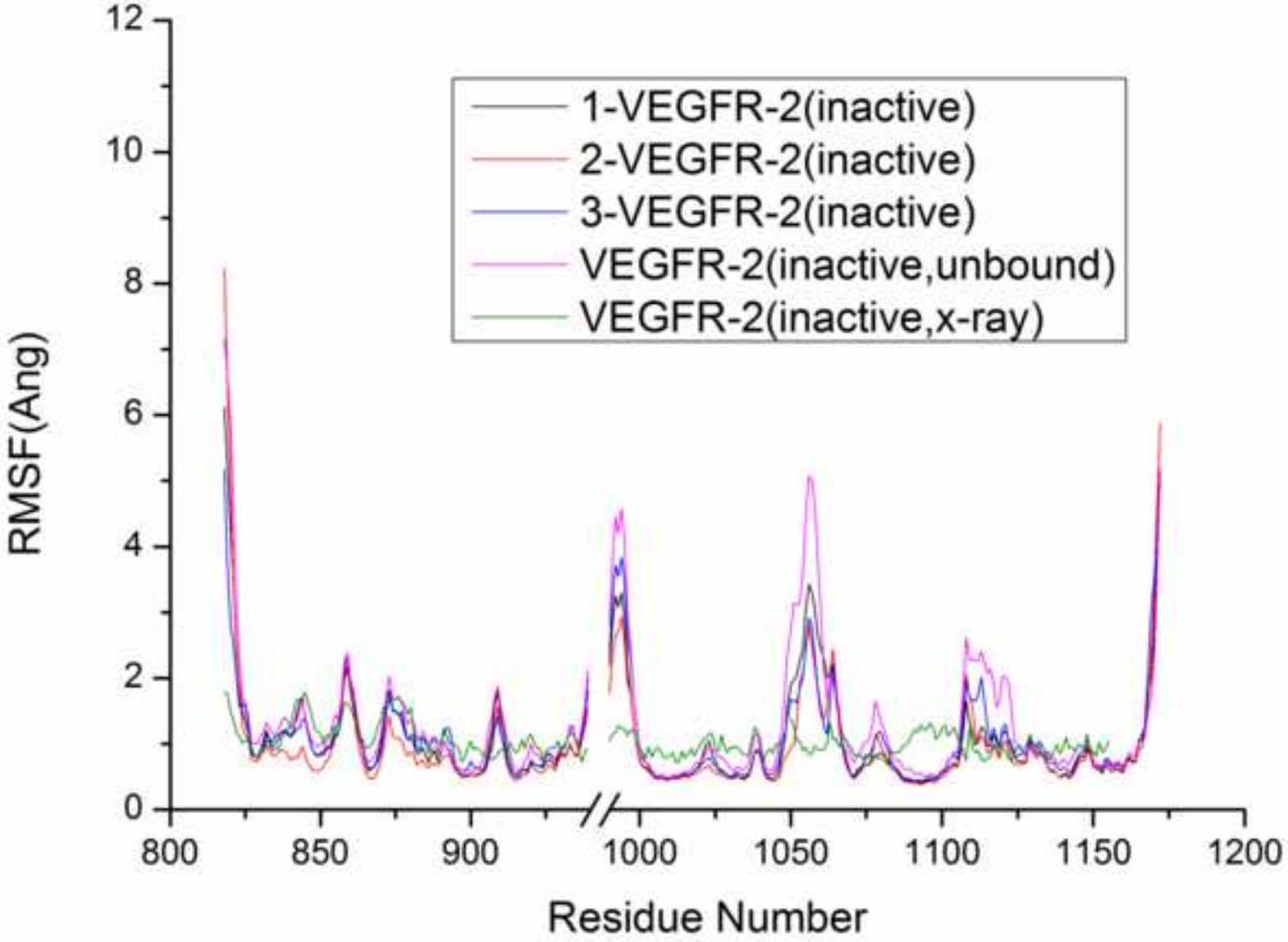
1-VEGFR-2(inactive)
2-VEGFR-2(inactive)
3-VEGFR-2(inactive)
VEGFR-2(inactive,unbound)
VEGFR-2(inactive,x-ray)
RMSF(Ang)
Residue Number
0
2
4
6
8
10
12
800
850
900
1000
1050
1100
1150
1200

Fig 5(a)

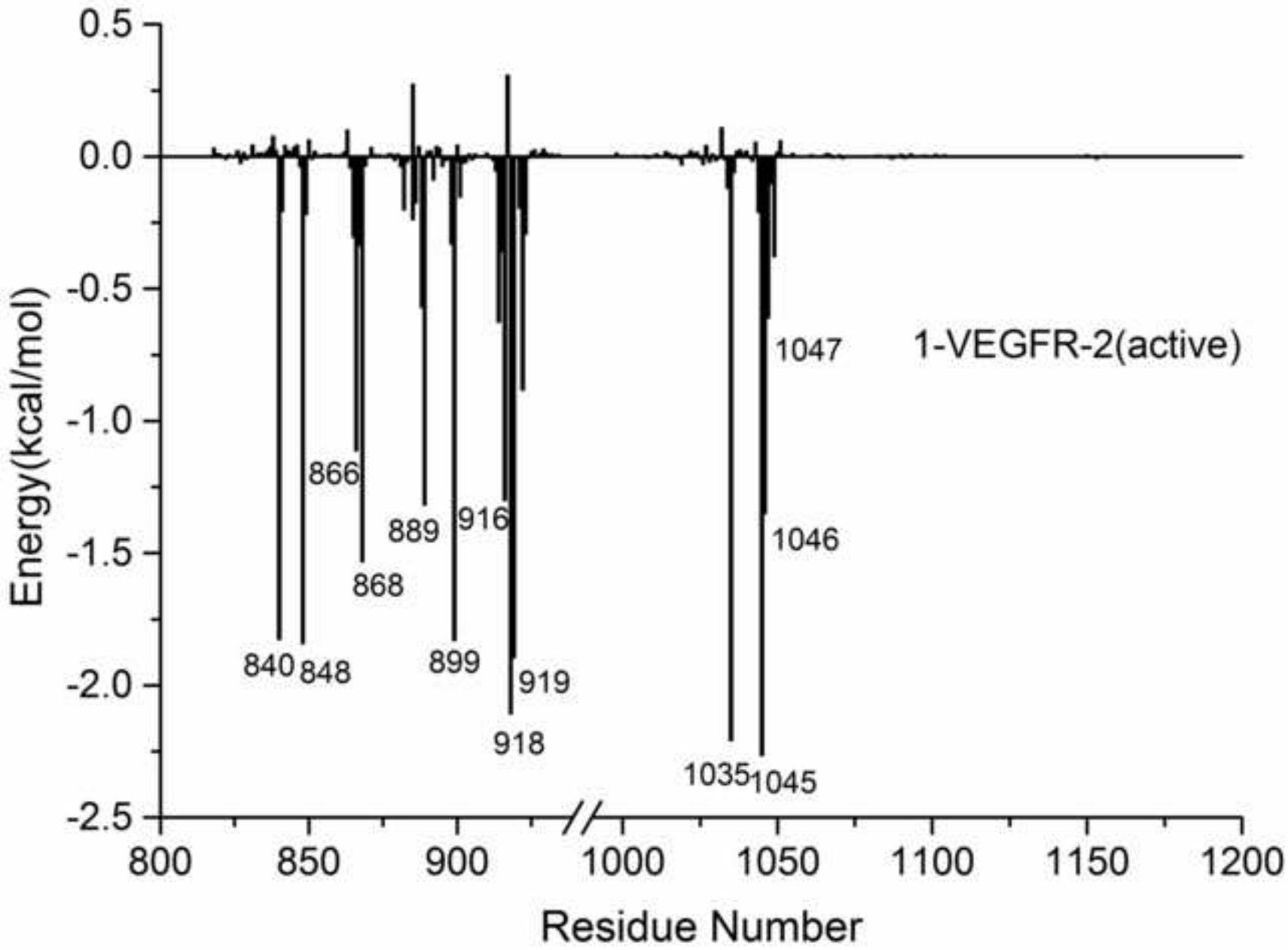
0.5
0.0
-0.5
-1.0
-1.5
-2.0
-2.5
Energy(kcal/mol)
800
850
900
1000
1050
1100
1150
1200
Residue Number
1-VEGFR-2(active)
840
848
866
868
889
899
916
918
919
1035
1045
1046
1047

Fig 5(b)

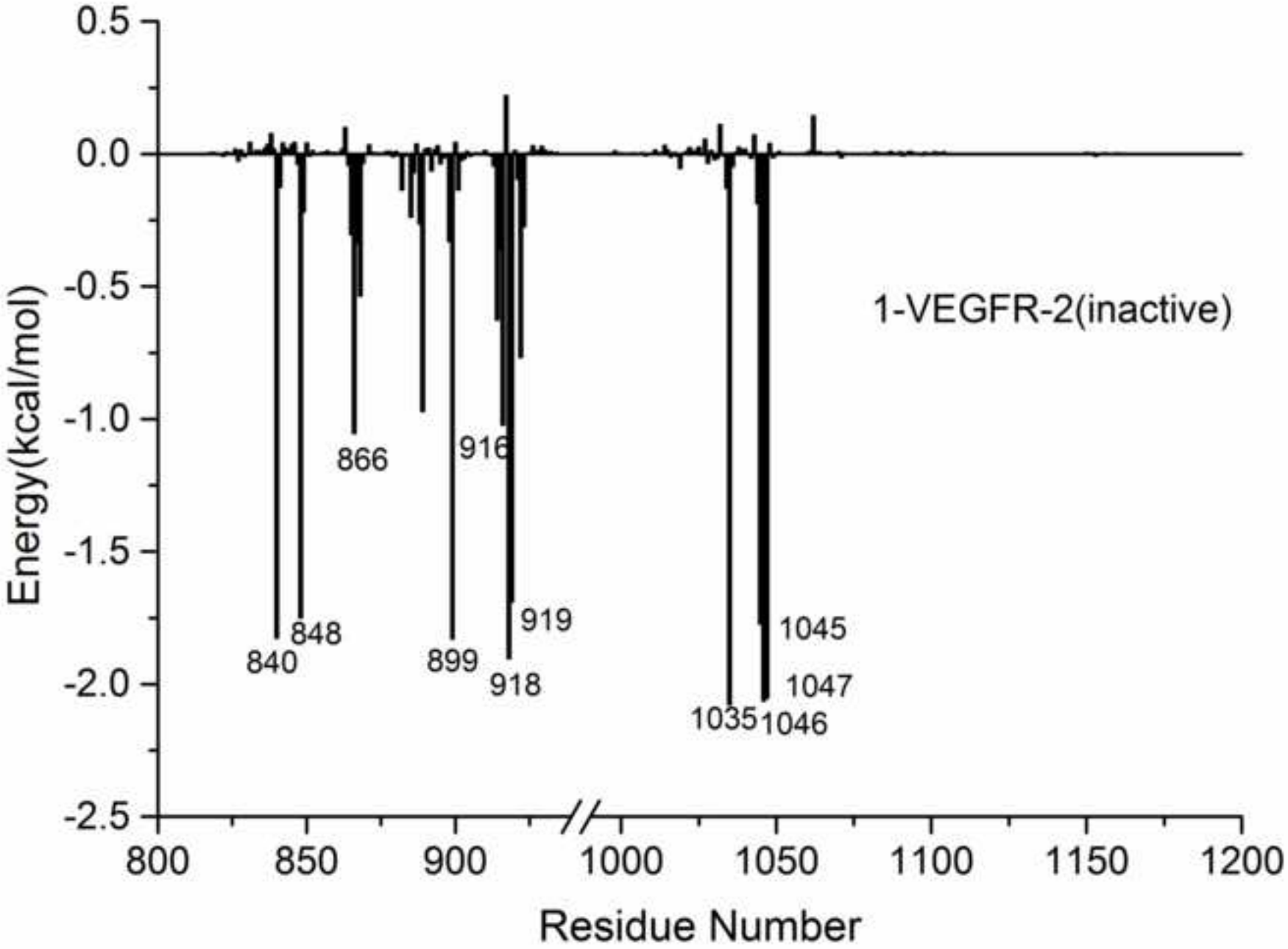
0.5
0.0
-0.5
-1.0
-1.5
-2.0
-2.5
Energy(kcal/mol)
1-VEGFR-2(inactive)
840
848
866
899
916
918
919
1035
1045
1046
1047
800
850
900
1000
1050
1100
1150
1200
Residue Number

Fig 5(c)

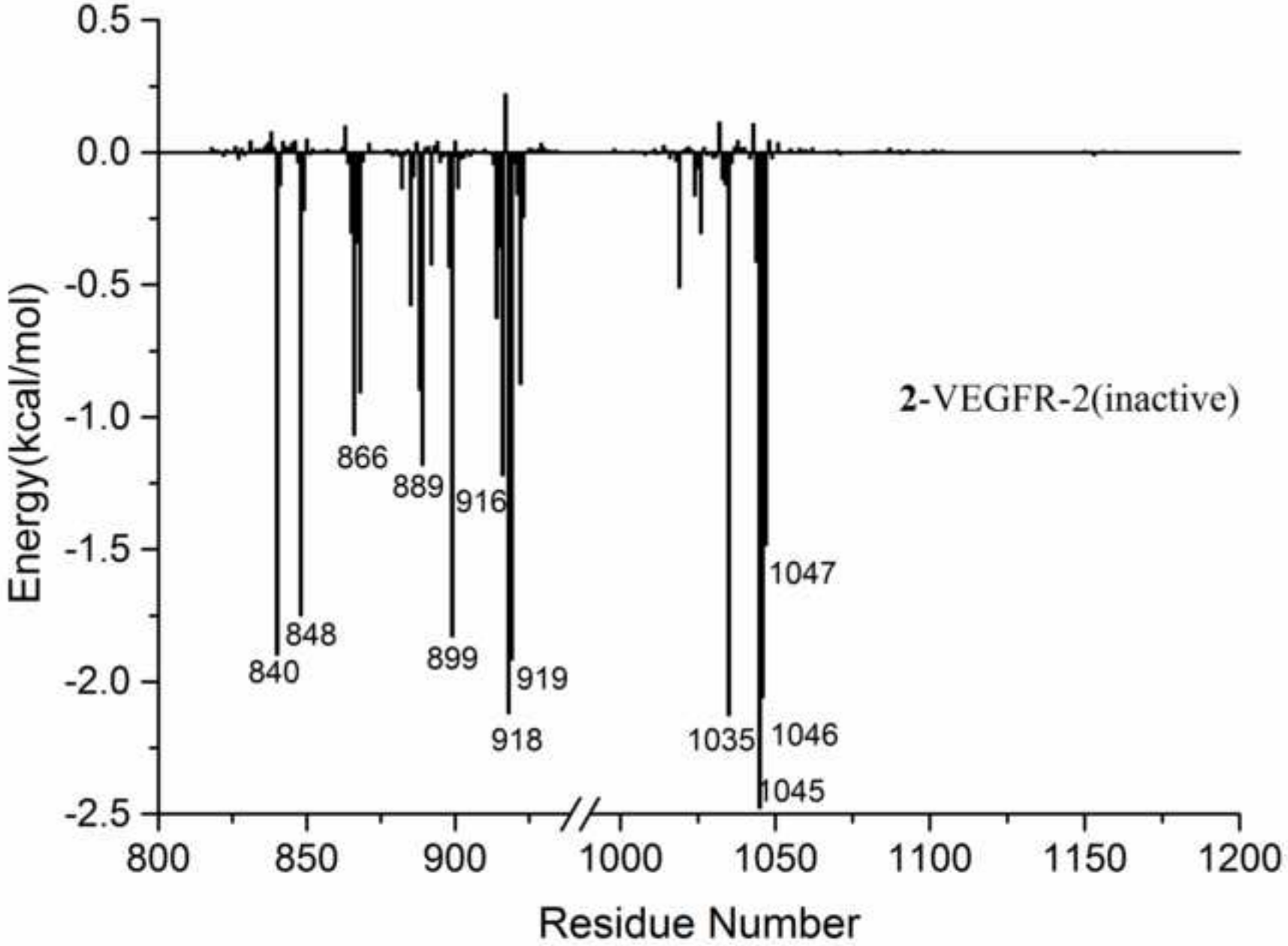
0.5
0.0
-0.5
-1.0
-1.5
-2.0
-2.5
Energy(kcal/mol)
800
850
900
1000
1050
1100
1150
1200
Residue Number
2-VEGFR-2(inactive)
840
848
866
889
899
916
918
919
1035
1045
1046
1047

Fig 5(d)

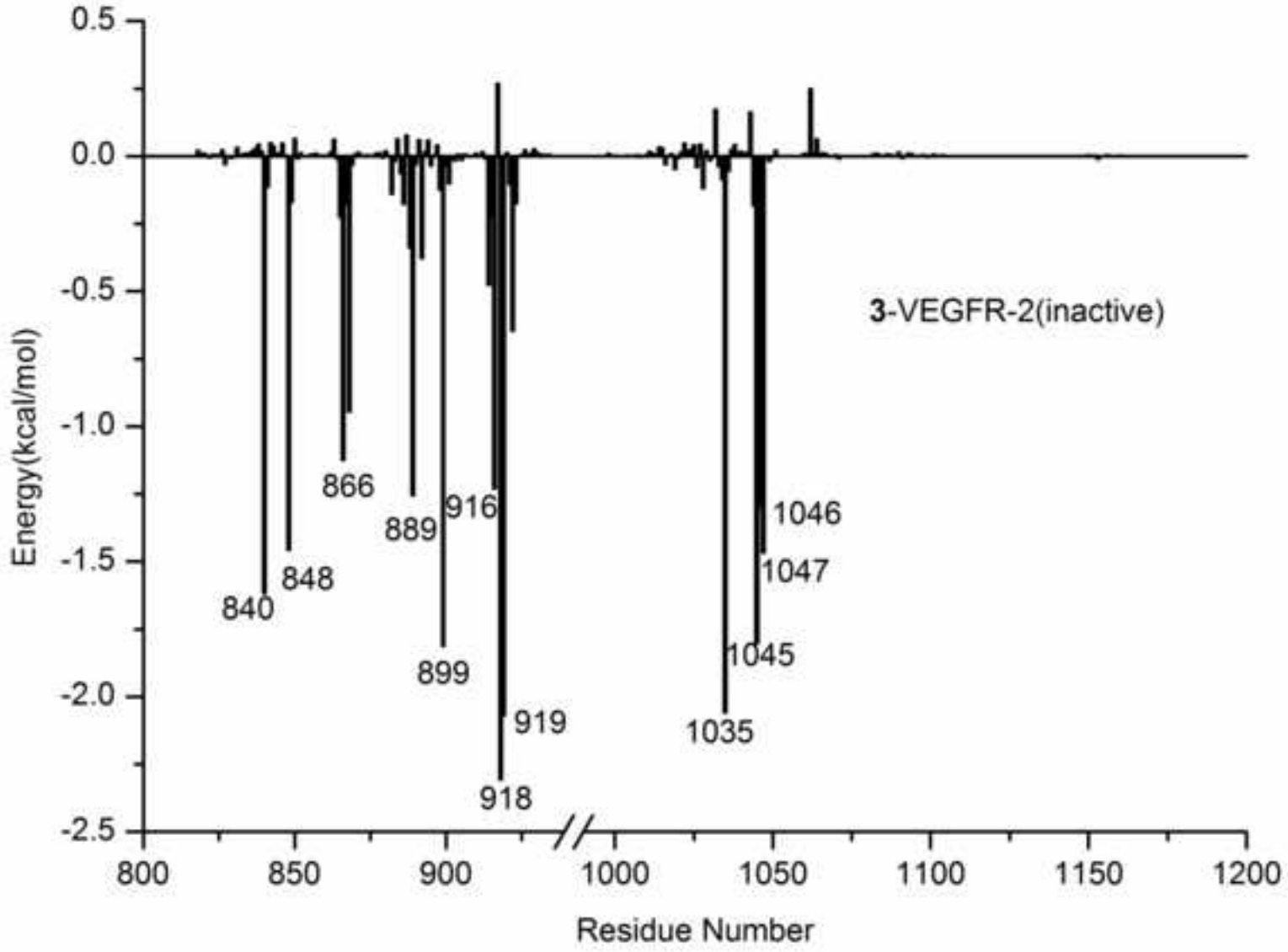
0.5
0.0
-0.5
-1.0
-1.5
-2.0
-2.5
Energy(kcal/mol)
3-VEGFR-2(inactive)
840
848
866
889
899
916
918
919
1035
1045
1046
1047
800
850
900
1000
1050
1100
1150
1200
Residue Number

Fig 6

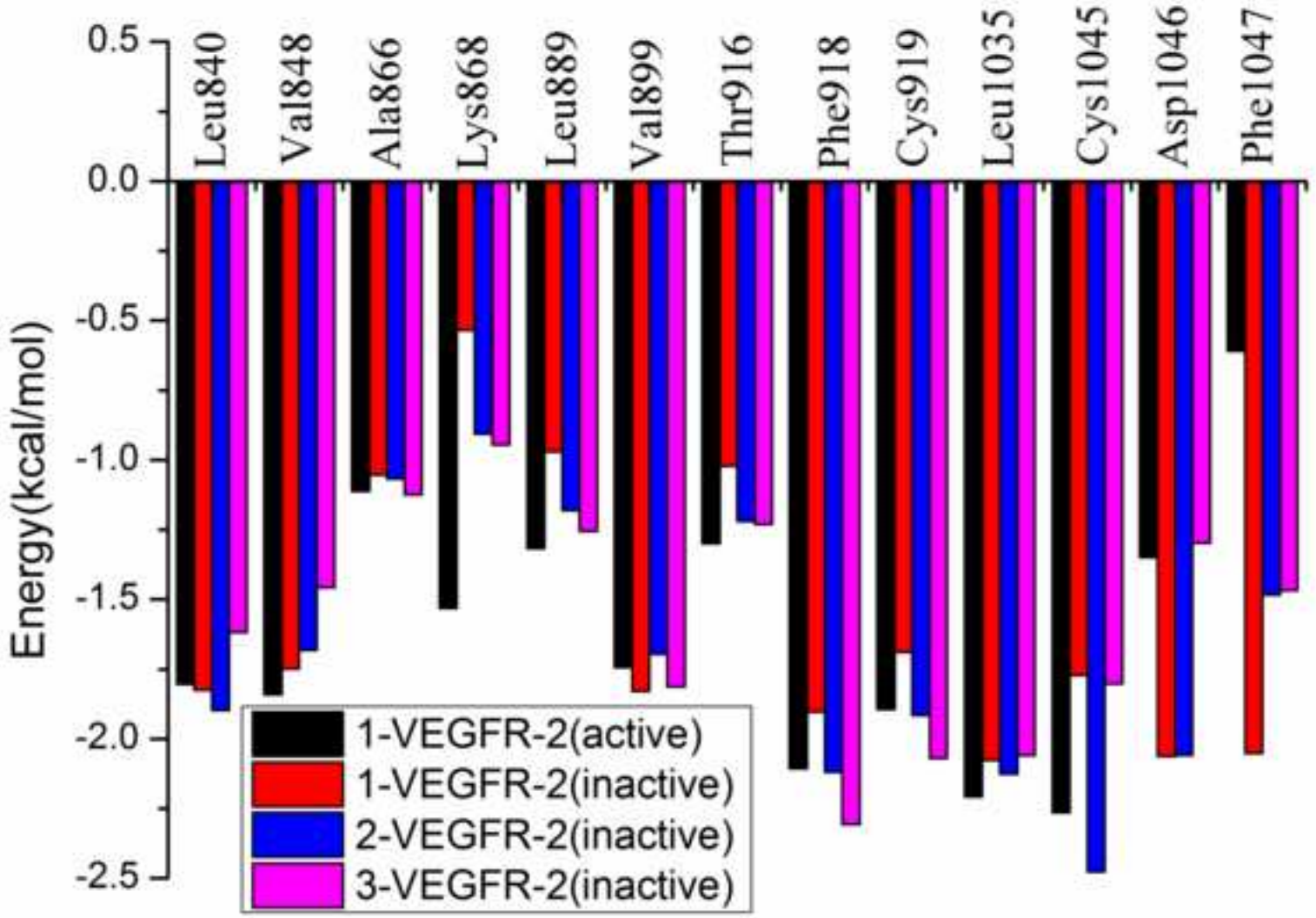
Leu840
Val848
Ala866
Lys868
Leu889
Val899
Thr916
Phe918
Cys919
Leu1035
Cys1045
Asp1046
Phe1047
0.5
0.0
-0.5
-1.0
-1.5
-2.0
-2.5
Energy(kcal/mol)
1-VEGFR-2(active)
1-VEGFR-2(inactive)
2-VEGFR-2(inactive)
3-VEGFR-2(inactive)